1 **Cloud phase and macrophysical properties over the Southern Ocean during**

2 **the MARCUS field campaign**

4 Baike Xi[1], Xiquan Dong[1], Xiaojian Zheng[1], and Peng Wu[2]

6 [1]Department of Hydrology and Atmospheric Sciences, University of Arizona, Tucson, AZ, USA

7 [2]Pacific Northwest National Laboratory, Richland, WA, USA

9 **Correspondence:** Baike Xi (baikex@arizona.edu)

Abstract.

To investigate the cloud phase and macrophysical properties over the Southern Ocean (SO), the Department of Energy (DOE) Atmospheric Radiation Measurement (ARM) Mobile Facility (AMF2) was installed on the Australian icebreaker *Aurora Australis* during the MARCUS field campaign [41 to 69 ℃S; 60 to 160 ℃E] from October 2017 to March 2018. To examine cloud properties over the mid-latitude and Polar regions, the study domain is separated into northern (NSO) and southern (SSO) parts of the SO with a demarcation line of 60 °S. The total cloud fractions (*CF*s) were 77.9 %, 67.6 %, and 90.3 % for the entire domain, NSO and SSO, respectively, indicating that higher *CF*s were observed in the Polar region. Low-level clouds and deep convective clouds are the two most common cloud types over the SO.

A new method was developed to classify liquid, mixed-phase and ice clouds in single-layered low-level clouds (LOW) where mixed-phase clouds dominate with an occurrence frequency (*Freq*) of 54.5 %, while the *Freq* of the liquid and ice clouds were 10.1 % (most drizzling) and 17.4 % (least drizzling). The meridional distributions of low-level cloud boundaries are nearly independent of latitude, whereas the cloud temperatures increased ~8 K and atmospheric precipitable water vapor increased from ~5 mm at 69 °S to ~18 mm at 43 °S. The mean cloud liquid water paths over NSO were much larger than those over SSO. Most liquid clouds occurred over NSO with very few over SSO, whereas more mixed-phase clouds occurred over SSO than over NSO. There were no significant differences for ice cloud *Freq* between NSO and SSO. The ice particle sizes are comparable to cloud droplets and drizzle drops, and well mixed in the cloud layer. These results will be valuable for advancing our understanding of the meridional and vertical distributions of clouds and can be used to improve model simulations over the SO.

1. Introduction

The Southern Ocean (SO) is one of the cloudiest and stormiest regions on the Earth (Mace et al., 2009; Chubb et al., 2013). Over the SO, most of the aerosols are naturally produced via oceanic sources given the remote environment. The uncertainties of aerosol forcing caused by natural emissions have larger variances than anthropogenic emissions, especially the dimethyl sulfide (DMS) flux contributes significantly to the bias (Carslaw et al., 2013). The SO is a unique natural laboratory to address the natural aerosol emissions and their contributions to the biases because it has rich ecosystems and is remote to human activities (McCoy et al., 2015). However, we have limited knowledge about cloud formation processes within such clean environments and their associated aerosol and cloud properties. The unique nature of the SO region features low-level supercooled liquid and mixed-phase clouds, which is significantly different from the subtropical marine boundary layer (MBL) clouds where warm liquid clouds are dominant (Dong et al., 2014; Wu et al., 2020; Zhao et al., 2020), and also different to the Arctic mixed-phase clouds which are featured with the liquid-topped cloud layer with ice cloud layer beneath (Qiu et al., 2015).

Large biases in cloud amount and microphysics over the SO in the Coupled Model Intercomparison Project phase 5 (CMIP5) climate models result in a near 30 W m^{-2} shortwave radiation deficit at the top of the atmosphere (TOA) (Marchand et al., 2014; Stanfield et al., 2014, 2015), which further leads to unrealistic cloud feedbacks and equilibrium climate sensitivity (Bony et al., 2015; Stocker et al., 2013). Meanwhile, the efficiency of aerosol-cloud interaction (ACI) over the SO was found to be crucial for the models' sensitivities to the radiation budget. A new aerosol scheme in the Hadley Centre Global Environmental model can dampen the ACI and suppress negative clear-sky shortwave feedback, both of which contribute to a larger climate sensitivity (Bodas-Salcedo et a., 2019).

70   A climate sensitivity study using CMIP6 general circulation models (GCMs) shows much

71   higher temperature variations across 27 GCMs in response to doubled CO_2 than those in CMIP5,

72   which may have resulted from the decreased extratropical low-level cloud cover and cloud albedo

73   over the SO in CMIP6 (Zelinka et al., 2020). Low-level clouds are a key climate uncertainty and

74   can explain 50 % of the inter-model variations (Klein et al., 2017) because conversion from liquid

75   cloud droplets to ice cloud particles decreases the cloud albedo and reduces the reflected shortwave

76   radiation at TOA. Models, however, have difficulties accurately partitioning the cloud phase

77   (Kalesse et al., 2016). The phase changes in mixed-phase clouds over the Arctic have proved to

78   affect the cloud lifetime and radiative properties significantly, that is, converting from ice cloud

79   particles to liquid cloud droplets may increase the cloud optical depth and the reflected shortwave

80   radiation at TOA (Morrison et al., 2012). In contrast, models that allow mixed-phase clouds to

81   glaciate rapidly can produce 30% more warming from doubling CO_2 (McCoy et al., 2014).

82   Phase transition processes have been investigated by several groups using both satellite and

83   ground-based measurements. For instance, Mace and Protat (2018) found that there are more

84   mixed-phase clouds over the SO measured from the ship than retrieved from CloudSat and

85   CALIPSO measurements because the satellites cannot accurately measure clouds below ~1 km.

86   Lang et al. (2018) used a model to investigate the clouds under post cold frontal systems and found

87   large biases in model simulations and concluded that the cloud cover and radiative biases over the

88   SO are highly regime dependent. Of all cloud types, low-level clouds are primarily responsible for

89   the biases in the model simulations due to the lack of reliable measurements, which leads to a poor

90   understanding of the conditions where these clouds form and the phase(s) that result. In other

91   words, a physical representation of clouds, especially for low-level clouds, is unclear but truly

92   necessary for improving model simulations. Therefore, reliable observations of the cloud macro-

93   and micro-physical properties from ground-based active and passive remote sensors are crucial for

94   the improvement of model simulations.

95   Previous studies show that cloud phase is primarily dependent on cloud temperature, and the

96   transition from one cloud phase to another will modify the cloud optical properties, which further

97   affects the radiation budgets (Hu et al., 2010; Intrieri et al., 2002; Morrison et al., 2012). Based on

98   satellite observations and retrievals, Hu et al. (2010) found that supercooled liquid water (SLW)

99   clouds are most common in the low-level clouds over the SO, where 80% of low-level clouds

100   contain SLW in a wide range of cloud temperatures from 0°C to −40°C. The formation of SLW

101   clouds is usually related to strong boundary layer convection. However, when ice nuclei exist in

102   the mixed-phase clouds, the ice particles can grow quickly and become bigger through consuming

103   supercooled liquid water drops. The SLW is inherently unstable due to the higher vapor pressure

104   over liquid than over ice and the quicker vapor deposition on ice particles than on liquid droplets

105   (Intrieri et al., 2002). As the supercooled liquid cloud droplets glaciate to ice particles, the cloud

106   layer becomes darker because the ice particles scatter less shortwave radiation and absorb more

107   radiation in the near IR wavelength regime. It is unclear, however, what role these ice particles

108   play in the low-level clouds over the SO, which includes the impact on drizzle development.

109   During HIAPER Pole-to-Pole Observation (HIPPO) campaigns, Chubb et al. (2013) found that

110   there are rarely ice particles in non-drizzling and light drizzling clouds over the SO, which may

111   imply that the ice particles in the mixed-phase clouds may modulate the drizzle formation.

112   To investigate the aerosol and cloud properties over the SO, a field campaign called the

113   Measurements of Aerosols, Radiation, and Clouds over the Southern Ocean (MARCUS) was

114   conducted using the ship-based measurements between Hobart, Australia, and the Antarctic during

115   the period October 2017-March 2018. The Department of Energy (DOE) Atmospheric Radiation

Measurement (ARM) Mobile Facility (AMF2) was installed on the Australian icebreaker *Aurora Australis,* which voyaged from Hobart, Tasmania to the Australian Antarctic stations of Casey, Mawson, and Davis, as well as Macquarie Island as illustrated in Fig. 1. Another field campaign, called South Ocean Clouds, Radiation, Aerosol Transport Experimental Study (SOCRATES) field campaign was conducted during austral summer from January 15 to February 26, 2018. In this study, the aircraft in-situ measurements during SOCRATES are used as the reference for the analysis. The SOCRATES domain is shown in the black dotted rectangle box in Fig. 1. The objectives of the MARCUS campaign are to investigate the vertical distribution of boundary layer clouds and reveal the reasons why the mixed-phase clouds are common in the warm season (McFarquhar et al., 2016; McFarquhar et al., 2021). Our study will focus on cloud macrophysical properties and cloud phase along the shiptracks during MARCUS.

MARCUS ship-based instruments include AMF2 cloud radar, lidar, microwave radiometer, micropulse lidar, radiosonde sounding, precision solar pyranometer and precision infrared radiometer, as well as aerosol sensors. Through these comprehensive observations over the SO, we are tentatively answering the following three scientific questions:

(1) What is the total cloud fraction over the SO during MARCUS, as well as vertical and meridional variations in cloud fraction?

(2) What are the dominant cloud types over the SO, their associated cloud phase and macrophysical properties, as well as their vertical and meridional distributions?

(3) What are the vertical and meridional distributions of the low-level clouds over the SO?

This manuscript is organized as follows: the data and method and introduced in section 2. The statistical results for all clouds during MARCUS are summarized in section 3. The low-level cloud

138   phase and macrophysical properties are described in section 4, followed by a summary and

139   conclusions in section 5.

140   **2. Data and Method**

141   **2.1 Ship-based measurements used in this study**

142   The AMF2 instruments, measurements, and their corresponding uncertainties and references

143   are listed in Table 1. Because AMF2 was designed to support shipboard deployments, the baseline

144   suite of instruments are marine-focused, including the 95-GHz W-band cloud radar (WACR),

145   ceilometer, micropulse lidar (MPL), microwave radiometer (MWR), aerosol observation system

146   (AOS), meteorological measurements (MET, includes the following data: temperature, pressure,

147   specific humidity, wind direction and speed) on the ship, rain gauge and the radiosonde soundings.

148   The combined cloud radar and ceilometer measurements can provide the cloud boundaries as long

149   as there are no optically thin clouds and the cloud-base heights (H_{base}) are not greater than the

150   upper limit (7.7 km) of the ceilometer. The micropulse lidar will be used to identify optically thin

151   clouds and the clouds with $H_{base} > 7.7$ km. A previous study has shown that these additional clouds

152   detected by the micropulse lidar can be a non-negligible supplement to the total cloud fraction

153   (Mace et al., 2021). A detailed description of the instruments and the cloud parameters during

154   MARCUS can be found in Mace et al. (2021) and McFarquhar et al. (2016 and 2021).

155   In order to accurately estimate the cloud temperatures, we adopted a linear interpolation

156   method based on the daily balloon soundings (4 to 5 times per day) to achieve a better temporal

157   resolution of the vertical profiles of temperature, pressure, and specific humidity. The method

158   considers MET measurements to ensure vertical continuity and adjacent soundings for temporal

159   continuity. Using these interpolated atmospheric profiles, cloud temperatures can be obtained at a

160   5-min temporal resolution.

161   The cloud liquid water path (*LWP*) and atmospheric precipitable water vapor (*PWV*) are

162   retrieved based on a physical-iterative algorithm using observations of the microwave radiometer

163   brightness temperatures at 23.8 and 31.4 GHz with uncertainties ranging from 15 to 30 g m^{-2}

164   (Marchand et al., 2003). It is important to note that the brightness temperature biases switch signs

165   among different climatological regions because a threshold of 5 ℃ in cloud-base temperature was

166   used in their physical retrievals. Since the retrieved LWP and PWV are based on the MWR

167   measured brightness temperatures at two frequencies, any biases on the brightness temperatures

168   will affect these retrievals. Therefore, we propose an extra step to determine the uncertainties

169   during MARCUS. Based on the temperature profiles, we can identify clouds that are not likely to

170   contain liquid (e.g., pure ice-cloud), then we can estimate the LWP uncertainty based on their

171   corresponding retrieved LWP values. From the probability density function (PDF_ analysis, the

172   LWP uncertainty is estimated as 10 g m^{-2} for MARCUS.

173   To determine the precipitation status, the AOS and rain gauge measurements were used to

174   determine whether rain is reaching the surface qualitatively, but not quantitatively in this study.

175   All the measurements were averaged over 5 minutes, except the radar reflectivity, Doppler velocity,

176   and spectrum width used in Section 4.3.

177   **2.2 Cloud type classification and single-layer low cloud phases**

178   A classification method developed in Xi et al. (2010) was used to categorize different types of

179   clouds using ARM radar-lidar estimated cloud base (H_{base}) and top (H_{top}) heights and cloud

180   thickness (ΔH). A brief description of the classification of cloud types is as follows (Table 1 and

181   Figure 6 in Xi et al., 2010). The single-layered low-level clouds (LOW) is the fraction of time

182   when low clouds with $H_{top} \leq 3$ km occur without clouds above them. Middle clouds (MID) range

183   from 3 to 6 km without any clouds below and above, while high clouds (HGH) have $H_{base} > 6$ km

184 with no cloud underneath. Other types of clouds are defined by different combinations of the above

185 three types, middle over low (MOL), high over low (HOL), high over middle (HOM), and the

186 cloud column through the entire troposphere is defined as HML. Three types, MOL, HOM, and

187 HML, include both contiguous and non-contiguous cloud layers, and their thicknesses may be

188 overestimated when clear layer(s) are present between any two cloud layers.

189   Furthermore, we used the measurements of interpolated sounding, microwave radiometer

190 retrieved *LWP*, radar reflectivity, Doppler velocity and spectrum width to classify the cloud phase

191 in each radar range volume of low-level clouds during MARCUS. The detailed classification

192 method will be introduced in Section 4.1. We also used ERA-Interim reanalysis data to study the

193 environmental conditions during MARCUS. The lower tropospheric stability (LTS) is calculated

194 from the potential temperature difference between the surface and 700 hPa to assess the boundary-

195 layer stabilities when the low-level clouds appeared along the shiptracks. The relative

196 contributions of mixed-phase, liquid and ice clouds to the single-layered low-level clouds as well

197 as their drizzling status are also analyzed in this study. The latitudinal and longitudinal variations

198 of the single-layered low-level clouds as well as their vertical distributions are further explored in

199 this study.

200   **3. Statistical results for all clouds during MARCUS**

201   The occurrence frequencies of total cloud cover and different types of clouds and their

202 associated properties over the entire study domain during MARCUS are presented in Figs. 2 - 4.

203 In order to examine the cloud properties over the mid-latitude and Polar regions, we separate the

204 SO domain into northern (NSO, north of 60°S) and southern (SSO, south of 60°S) parts using a

205 demarcation line of 60ºS. A total of 2,447 hours cloud samples were collected during MARCUS

206 in this study, in which 1,181 hours of samples were located in the NSO and 1,266 hours of samples

207   were collected from the SSO. It is important to note that adding micropulse lidar measurements

208   increased the total samples of non-liquid-containing clouds by ~20% because micropulse lidar is

209   more sensitive to optically thin clouds than cloud radar. However, micropulse lidar signals are

210   usually attenuated and cannot provide a meaningful signal when the liquid cloud layer is thicker

211   than a couple of hundred meters (Sassen, 1991).

212   Figure 2 shows the vertical distributions of total cloud cover over the entire domain, as well as

213   over NSO and SSO. For the vertical distributions, the occurrence frequencies of total cloud

214   increase from the first radar gate (~ 226 m) to ~700 m, then monotonically decrease with altitude

215   with a few small increments at different levels, especially over SSO. Comparing the occurrence

216   frequencies of total cloud between NSO and SSO, we can draw the following conclusions. 1) The

217   SSO has more cloudiness than the NSO under 7 km, while the NSO has more cloudiness than the

218   SSO above 7 km. 2) Below 3 km, the occurrence frequencies of clouds over the NSO decrease

219   dramatically from 37 % at an altitude of ~700 m to 16 % at 3 km and from 45 % to 28 % over the

220   SSO, which is similar to the vertical distributions of the low-level clouds over some Northern

221   Hemisphere mid-latitude regions, such as Eastern North Atlantic (ENA, Dong et al., 2014). The

222   occurrence frequencies measured during MARCUS are much lower than these shown in Fig. 8 of

223   Mace et al., (2009) throughout the entire vertical column between the same range of latitudes,

224   especially, the occurrence frequencies during MARCUS are almost half of those measured by

225   CloudSat and CALIPSO from 1 to 3 km. The reason has been explained in Xi et al., (2010), that

226   is, a comparison of occurrence frequencies between measurements of two different platforms can

227   only be performed under an equivalent spatial-to-temporal resolution. In other words, our results

228   were calculated under 5-min temporal resolution, and the results in Mace et al., (2009) were

229   statistically in the 2º gridbox. Therefore, the comparison between these two results is not

230   reasonable. To make a fair comparison, one has to know the cloud amount at each area or time

231   step, then the product of amount and frequency is independent of either temporal and spatial

232   measurement.

233   To compare with other studies, we calculated the cloud fractions (CFs) of total and different

234   types of clouds. The total CFs were 77.9 %, 67.6 %, and 90.3 % for the entire domain, NSO and

235   SSO, respectively, indicating that 22.7 % more clouds occurred in the Polar region than in the mid-

236   latitude region. The total CF over the entire domain is very close to the 76 % calculated by Mace

237   and Protat (2018) using ship-based measurements during the Cloud, Aerosols, Precipitation,

238   Radiation and Atmospheric Composition (CAPRICORN) field experiment. The total CF over the

239   SSO is close to that estimated by using the complementarity of CALIOP lidar aboard CALIPSO

240   and CPR aboard CloudSat (DARDAR version 2 data) from Listowski et al. (2019).

241   Figiure 3 shows the occurrence frequencies of categorized clouds and their cloud boundaries

242   using the maximum H_{top} and the minimum H_{base} if there are two or more layers in each 5-min

243   sample. For example, the mean H_{base} and H_{top} for single-layered low-level (LOW) are 0.92 km and

244   1.62 km, respectively, listed in Table 2, which are the average values of min H_{base} and max H_{top} in

245   LOW category. As illustrated in Fig. 3a, the single-layered low-level (LOW), deep cumulus or

246   multi-layered (HML), and MOL clouds are the three dominant types of clouds over the SO.

247   Comparing the clouds between NSO and SSO, all types of clouds in SSO have higher frequency

248   of occurrence than those in NSO except HOL. The differences range from less than 1 % (LOW)

249   to more than 10 % (MOL). Comparing the clouds over mid-latitude oceans between the two

250   hemispheres, i.e., between NSO and ARM ENA site (Dong et al., 2014), we find: (1) The total

251   cloud fractions (CFs) are close to each other (67.6 % over NSO vs. 70.1 % at ARM ENA); (2)

252   LOW CFs are 22.9 % vs. 27.1 %, which is the dominant type of cloud in both regions; and (3)

253   Both MOL and HML clouds, including underneath low clouds, are 14.2 % and 16.5 % over NSO,

254   much higher than those (4.2 % and 12.1 %) at ARM ENA site, indicating that there are more MOL

255   and deep convective clouds over NSO than over ENA.

256   Figure 3b shows the vertical locations of different types of cloud layers, which represent the

257   mean H_{top} and H_{base} listed in Table 2 for any type of cloud. Nearly all H_{top} and cloud thickness (*ΔH)*

258   values over NSO are higher or deeper than those over SSO, presumably due to stronger solar

259   radiation and stronger convection over NSO. H_{base} values basically followed their cloud-top

260   counterparts with a couple of exceptions. These cloud macrophysical properties are closely

261   associated with large-scale dynamic patterns and environmental conditions. By analyzing the

262   ERA-Interim reanalysis (not shown), the 850 hPa geopotential heights show persistent westerlies

263   with slightly higher geopotential heights over the northwest corner of the domain, which may

264   closely relate to the higher H_{top} over NSO than over SSO. Furthermore, the boundary layer over

265   NSO is relatively more stable than over SSO based on lower troposphere stability (LTS) analysis

266   (12.2-15.32 K over NSO vs. 11.48-13.29 K over SSO).

267   When we plot the probability density functions (PDFs) of cloud *LWP*s for different types of

268   clouds, we find that the PDFs of *LWP*s for HGH and HOM peak are less than 10 g m^{-2}. These

269   results make physical sense because HGH clouds should not contain any liquid droplets, and most

270   HOM clouds, especially those over SSO, should be ice phase dominant. In addition, the 10 g m^{-2}

271   of *LWP* is close to the uncertainty of the *LWP* retrieval in Marchand et al., (2003). Therefore, this

272   value is used as a threshold for all types of clouds, which leads to less than one percent reduction

273   of the total samples. As shown in Fig. 4a, the *LWP*s (> 10 g m^{-2}) for all types of clouds are much

274   higher over NSO than over SSO because the low-level and MOL clouds in the mid-latitudes

275   contain more liquid water than those in Polar regions. The mean *LWP*s for liquid containing low-

276   level and middle-level clouds over NSO, i.e. LOW, MID and HOL, range from ~130 to 150 g m$^-$

277   ^{2}, while the mean LWPs for MOL and HML are two times higher (~270 g m^{-2}) than the mean LWP

278   of LOW, MID and HOL. Note that the mean LWPs for most types of clouds over the SSO are

279   much lower than those over the NSO, except for the LOW clouds.

280   The occurrence frequencies of LWPs (> 10 g m^{-2}) over NSO and SSO contradict their cloud

281   LWP values as demonstrated in Fig. 4b. To further investigate the amount of available precipitable

282   water vapor (PWV), we found that mean PWV values in SSO are at least 2 to 3 times less than

283   those in NSO for same types of clouds (figure not shown). Note that the samples of MID, HGH,

284   and HOM clouds are excluded from this study when they have LWPs less than 10 g m^{-2}, since

285   these low LWPs are within the retrieval uncertainty of cloud LWP and hence may not contain any

286   liquid cloud droplets. The higher LWPs, larger cloud droplets, drizzle drops and ice particles, and

287   greater drizzling occurrence frequencies over NSO (which is discussed later) will lead to the quick

288   dissipation of clouds over NSO. In contrast to NSO, the SSO cloud LWPs and particle sizes are

289   much smaller with less drizzling events, which increases cloud lifetime relative to NSO. The 67.6 %

290   and 90.3 % CFs over NSO and SSO provide strong evidence for this argument. We can draw the

291   following conclusions by comparing the cloud macrophysical properties between NSO and SSO

292   in Figs. 3 and 4. The LOW fraction, thickness, and LWP over NSO and SSO are comparable to

293   each other. For other types of clouds, cloud thicknesses are similar to each other or slightly deeper

294   over NSO, but the cloud LWPs over NSO are much larger than those over SSO, resulting in more

295   precipitation events over NSO. As pointed out in Albrecht (1989), more precipitation events may

296   reduce the cloud lifetime. This argument is consistent with the results shown in Figs. 2 and 3a for

297   all clouds except for HOL. Cloud lifetimes over NSO are shorter than those over SSO, which leads

298   to lower CFs over NSO than over SSO.

299   Table 2 provides a summary of the mean, standard derivation, minimum and maximum for

300   cloud boundaries, LWP and the percentage of multi-layered cloud for each cloud type over the SO.

301   Non-contiguous (multi-layer) clouds over the SO occur very frequently, especially for HOM and

302   HML. The *LWP* for single-layered clouds is greater than that for multi-layered clouds. The *LWP*

303   for single-layered HML almost doubles that for multi-layered HML.

304   **4.   Single-layered low-level clouds**

305   As discussed in Section 3, single-layered low-level clouds (LOW) are the dominant cloud type

306   in both northern (NSO) and southern (SSO) parts of the SO. Figs. 3 and 4 further reveal that LOW

307   cloud type is the only one having comparable *CF*, cloud, thickness, *LWP* over both NSO and SSO.

308   This warrants further study: Are the cloud phases, properties, and vertical and meridional

309   variations of LOW clouds over these two regions similar to each other or significantly different?

310   **4.1. Cloud phase**

311   In this study, cloud boundaries are determined by combining cloud radar, ceilometer and

312   micropulse lidar measurements at a temporal resolution of 5-min. The cloud phase, liquid water

313   droplets or ice particles, are determined in each radar range volume. A flow chart for classifying

314   the phases of single-layered low-level clouds is drawn in Fig. 5. The determination of warm liquid

315   clouds is straightforward using both cloud-base (T_{base}) and -top (T_{top}) temperatures greater than 0

316   °C, and cloud *LWP*s greater than the threshold (10 g m^{-2}). The determination of supercooled liquid

317   clouds is slightly complicated. When either T_{base} or T_{top} is below 0° C, and cloud *LWP*s are greater

318   than the threshold, the radar Doppler spectrum width (*WID*) and velocity (V_{d}) are used for the

319   determination of supercooled liquid water clouds. If the majority (10 seconds of original radar

320   measurements) of *WID* within a 5-min period are less than 0.4 m s^{-1} and V_{d} are equal to or less than

321   0.0 m s^{-1} (updrafts) in the volume, then this range volume is defined as supercooled liquid clouds.

322   Mixed-phase clouds are determined when the median (calculated from 10 seconds of original
323   radar measurements) of *WID* is greater than 0.4 m s^{-1} or V_d is greater than 0.0 m s^{-1} (downdrafts)
324   due to the existence of large ice particles in the clouds. If cloud *LWP* is below the threshold, then
325   it is defined as an ice cloud, otherwise it is defined as a mixed-phase cloud. It is worth mentioning
326   that large ice particles, which grow through vapor deposition or rime processes, dominate the radar
327   reflectivity and are heavier than cloud droplets. Therefore, these large ice particles not only
328   broaden the spectrum width but also have relatively large fall speeds.

329   To further evaluate our classification method, we compared the classified mixed-phase and ice
330   clouds with the micropulse lidar linear depolarization ratios (*LDR*) as an extra measure. The *LDR*
331   ranges follow the method in Shupe et al., (2005), which are $0.11 < LDR < 0.15$ for mixed-phase
332   clouds, and $LDR > 0.15$ for ice clouds as listed in Table 1. Table 3a shows the quantitative
333   comparison of the cloud phase identifications between these two classification methods. The
334   numbers represent the counts of each matched 5-min sample, where the diagonal numbers indicate
335   that both methods are identifying the same type of cloud phase. In general, the two methods have
336   89 % agreement on the phase identification. Secondly, we performed the phase classification
337   directly from microphysical probes onboard G-1 aircraft during SOCRATES and treated them as
338   'ground-truth' (Mohrmann et al., 2021). Since the in-situ cloud microphysical measurements can
339   tell us the phase of the cloud, it allows us to see the percentage variations of cloud phase, by
340   changing integration time of in-situ sampling to mimic what the radar may observe the cloud for
341   each range volume. Table 3b shows possible cloud phase partitionings that may be detected by
342   cloud radar. As sampling time increases from 1 second to 30 seconds, more mixed-phase clouds
343   and fewer single-phase clouds can be observed.

344   Figure 6 shows the determination of mixed-phase and ice clouds through combined

345   measurements of radar reflectivity and spectrum width, lidar LDR and backscatter, and cloud LWP.

346   For the classified ice clouds, cloud LWPs are lower than 10 gm^{-2} (Fig. 6f), most of the Doppler

347   spectrum widths range from 0.08 to 0.16 m s^{-1} (Fig. 6b) and the *LDR* ratios (Fig. 6d) can be greater

348   than ~0.15, representing a narrow range of ice particle size distribution with higher *LDR* ratios.

349   For the classified mixed-phase clouds, cloud LWPs are greater than 10 gm^{-2} and most of the

350   Doppler spectrum widths range from 0.15 to 0.5 m s^{-1}, representing a broad particle size

351   distribution resulting from the mixture of liquid droplets and ice particles. An interesting result

352   occurs where both *LDR* signals (>0.2) and LWPs are much higher during the drizzling periods

353   (Fig. 6a), indicating a mixed-phase cloud with cloud droplets within the cloud layer and large

354   liquid drizzle drops and ice crystals below cloud base.

355   Based on the Doppler velocity, the mode values for both mixed-phase and ice clouds occur at

356   ~ 0.5 m s^{-1}, where the ice particles are dominant in both types of clouds. The broader particle size

357   distribution with lower *LDR* ratios for mixed-phase clouds and narrower particle size distribution

358   with higher *LDR* ratios for ice clouds further corroborate that the classified results from this study

359   are consistent with the traditional micropulse lidar *LDR* method.

360   It is important to note that the micropulse lidar signals are usually attenuated and cannot

361   provide a meaningful signal when the liquid cloud layer is thicker than a couple of hundred meters

362   (Sassen, 1991). Arctic mixed-phase clouds are typical with the liquid-dominant layer on the top of

363   the mixed-phase clouds and the ice-dominant layer underneath. The ceilometer-derived cloud-base

364   height represents the base of the liquid-dominant layer near the cloud top, while MPL-derived

365   cloud-base height represents the base of the lower ice-dominant layer (Qiu et al., 2015; Shupe,

366   2007; Shupe et al., 2005). Over the Arctic, the micropulse lidar signals can penetrate through the

367   ice-dominant layer to the liquid-dominant layer. However, the mixed-phase clouds over the

368   Southern Ocean are totally different from those over the Arctic region: they are well mixed (liquid

369   droplets and ice particles) from cloud base to cloud top, which is found in this study. Thus, the

370   micropulse lidar signals can be attenuated in the mixed-phase clouds over the Southern Ocean.

371   Statistical results show that 43 % of micropulse lidar signals were attenuated during MARCUS

372   compared to our classified results.

373   This classification method is further supported by the onboard cloud radar measurements

374   during the Southern Ocean Clouds Radiation Aerosol Transport Experimental Study (SOCRATES,

375   not shown). In that campaign, the reflectivity measurements were usually greater, and the spectrum

376   widths were much wider when the aircraft observed large ice particles compared to the time

377   periods when liquid cloud droplets were observed. Although the wider spectrum widths might be

378   caused by Doppler broadening of the moving aircraft, further analysis shows that the onboard radar

379   sends the signals (assuming the time of transmitted and received signals is short enough comparing

380   to aircraft speed) in the perpendicular to the movement of the aircraft, that is, there is no relative

381   movement between radar signals and clouds. Thus, the onboard radar spectrum width

382   measurements should be not significantly impacted by Doppler broadening (relative movement in

383   the same direction).

384   In this study, a total of 6,934 5-min single-layered low-level cloud samples were determined

385   using our classificaiton method, including 697 liquid cloud samples, 3,777 mixed, 1,205 ice, and

386   1,255 'OTHER' clouds. The category of 'OTHER' clouds represents more than one phase in each

387   column. Note that though the 'OTHER' is also mixed-phase cloud, it has different vertical

388   distribution of liquid compared to the 'mixed' cloud. It is also worth mentioning that about 5.5 %

389   of single-layered low-level cloud phases cannot be determined when the radar measurements were

390   not available during MARCUS, those were not accounted to "OTHER'.

391   Figure 7 (upper panel) shows the drizzling status for each categorized cloud type, i.e., no rain

392   (yellow-green), virga (brown) and rain (navy blue). The definition of drizzling status follows the

393   method in Wu et al., (2015, 2017) where there are radar reflectivity measurements below the

394   ceilometer/lidar determined cloud base. The major difference for drizzles in the studies of Wu et

395   al. (2015, 2017) and this study is that drizzle is liquid phase at ARM ENA site but could be both

396   liquid and ice phases in this study.

397   The percentages shown below the x-axis represent the portion of drizzling status in each type

398   of clouds, such as liquid, mixed-phase, ice and 'OTHER' clouds. Figure 7 (bottom panel) also

399   shows the percentages and vertical distributions of classified liquid, mixed-phase, ice, and

400   'OTHER' clouds for each column in the single-layered low-level clouds, represented by different

401   colors. After classification, the samples in each category are sorted by their H_{top}. In detail, Figure

402   7 demonstrates that the mixed-phase clouds dominate the single-layered low-level cloud category

403   with an occurrence frequency of 54.5 %. The 'OTHER' and ice clouds have similar occurrence

404   frequencies of 18.1 % and 17.4 %, respectively, while the liquid clouds have the lowest occurrence

405   frequency of 10.1 %. The liquid-topped mixed-phase clouds (included in 'OTHER'), which

406   frequently occur in the Arctic region (Qiu et al., 2015), are rarely found over the SO. The existence

407   of ice particles in mixed-phase clouds should strongly depend on the distribution of ice nuclei (IN),

408   whereas spatially unevenly distributed IN may result in the OTHER type of clouds.

409   Based on the results in Fig. 7, we draw the following conclusions. Most of the ice clouds are

410   without icy precipitation, and the percentages with virga and precipitation below the cloud base

411   are 12 % and 15 %, respectively. The percentages of non-drizzling, virga and drizzling mixed-

412   phase clouds are 50 %, 21 %, and 29 %. The liquid and 'OTHER' clouds have similar percentages,

413   they are 36 %, 25 % and 39 % for liquid clouds, and 35 %, 22 % and 44 % for 'OTHER' clouds.

414   For liquid and 'OTHER' clouds, the drizzling frequencies are independent of H_{top}. In contrast, for

415   mixed-phase and ice clouds, the drizzling frequencies strongly depend on $H_{top,}$ i.e., higher drizzling

416   frequencies occur mostly at higher H_{top}.

417   The properties of single-layered low-level clouds are summarized in Table 4. The liquid clouds

418   have the lowest H_{base} and H_{top} but more available water vapor than other types of clouds. Since the

419   'OTHER' clouds are a transitional stage among mixed-phase, liquid and ice clouds, they have the

420   highest H_{top}, deepest cloud layer and largest LWP. The ice clouds occur in relatively dry

421   environments and have the highest H_{base} at 1.218 km and thinnest cloud layer. The cloud variables

422   for mixed-phase clouds fall between Liquid and "OTHER". Since LWPs in mixed-phase clouds

423   have larger standard deviation, which implies that SLW is more common at higher LWPs and ice

424   is more common at lower LWPs.

425   **4.2. Meridional variations of cloud properties**

426   Figure 8 shows the meridional variation in single-layered low-level cloud properties during

427   MARCUS. As illustrated in Fig. 8a, the meridional distributions of $H_{base,}$ H_{top} and ΔH are nearly

428   independent of latitude, however, their corresponding temperatures (T_{base} and T_{top}) increased about

429   8 K from 69 $^{\circ}$S to 43 $^{\circ}$S, though there were slight fluctuations. These results suggest that the cloud

430   and sea surface temperatures have minimal impact on the cloud boundaries over the SO, which is

431   consistent with the findings in McFarquhar et al. (2016). The meridional variation of LWPs follows

432   those of T_{base} and T_{top}, with an increasing trend from south to north. It is important to point out that

433   a big drop in LWP at ~50 ºS results from fewer occurrences of low-level clouds there, indicating

434   that the cloud samples at some latitudes are not statistically significant. The atmospheric PWV

435   increased dramatically from ~ 5 mm at 69 $^{\circ}$S to ~18 mm at 43 $^{\circ}$S, presumably due to increased sea

436   surface and atmospheric temperatures.

437   Figure 9 shows the latitudinal and meridional distributions of categorized liquid, mixed-phase,

438   ice and 'OTHER' in single-layered low-level clouds over the SO during MARCUS. Each circle

439   represents the exact location and time along the ship track. Mixed-phase clouds occurred

440   everywhere over the SO during the MARCUS field campaign and became dominant in November,

441   December and February. Liquid clouds dominated in March, while ice clouds dominated in

442   January. The 'OTHER' clouds are a kind of transitional phase falling in between the mixed-phase

443   and ice/liquid clouds because there are no stand-alone occurrences in any month during MARCUS.

444   **4.3 Vertical distribution of cloud properties**

445   The vertical distributions of classified liquid, mixed-phase, and ice clouds in LOW category

446   are presented in Figs. 10-12. The focus of this section will be comparisons of cloud macrophysical

447   properties between the north (NSO) and south (SSO) regions of the domain. Figure 10a shows the

448   vertical distributions of liquid clouds, which were capped at ~ 1.6 km, mostly in the marine

449   boundary layer. The vertical occurrence frequencies are up to 27 % over NSO, while they were

450   less than 4 % over SSO, i.e., liquid clouds occurred fairly often over the mid-latitude region, but

451   very few occurred over the Polar region. On the contrary, the occurrence frequencies of mixed-

452   phase clouds between NSO and SSO are opposite to liquid clouds as illustrated in Fig. 10b, though

453   the differences are not so obvious. Mixed-phase clouds increased with altitude until ~1.6 km, then

454   decreased monotonically towards 3 km. The highest frequencies were ~37 % at 0.6 km over SSO

455   and ~27 % at 1.5 km over NSO. The vertical distributions of ice clouds are similar to those of

456   mixed-phase clouds (Fig. 10c), however, there were no significant differences between NSO and

457   SSO. It is worth mentioning that the vertical distributions of mixed-phased clouds over SO are

458   quite different to those from DOE ARM Northern Slope Alaska (NSA) site, where the low-level

459   mixed-phase clouds are commonly featured with a liquid-topped layer. (e.g., Qiu et al., 2015).

460   To further investigate the vertical distributions of classified liquid, mixed-phase, and ice clouds

461   over NSO and SSO, we plot the normalized vertical distributions (cloud base as 0, cloud top as 1)

462   of radar reflectivity, Doppler velocity and spectrum width in Figs. 11 and 12, respectively. In this

463   study, the threshold of -50 dBZ was used to determine the cloud boundary over the SO instead of

464   the threshold of -40 dBZ radar reflectivity used at the ARM ENA site (Dong et al., 2014). If we

465   used the threshold of -40 dBZ over the SO, then there would be only 73% cloud samples available.

466   If we used the threshold of -50 dBZ, then we would have 90.4% cloud samples, which gained

467   additional 17.4% on top of the -40 dBZ threshold. About 9.6% of radar reflectivities during

468   MARCUS are lower than -50 dBZ for all LOW cloud samples, but without ceilometer and MPL

469   lidar signals. Thus these 9.6% cloud samples were eliminated in Figs 11-12.

470   Figures 11a-11c represent the normalized vertical distributions of radar reflectivity, Doppler

471   velocity and spectrum width of liquid clouds. Liquid clouds had the lowest reflectivity near the

472   cloud top because of cloud-top entrainment., The reflectivity had a nearly constant median value

473   of ~ -22 dBZ from cloud top height (~ 0.8 for normalized height) of the cloud layer to the cloud

474   base. Most of the reflectivities were less than -15 dBZ, which is a threshold to distinguish cloud

475   droplets and drizzle drops in each radar range volume (Wu et al., 2020). Most of the Doppler

476   velocities were greater than 0.0 m s^{-1}, indicating that downwelling motion is dominant in liquid

477   clouds. The profiles of Doppler velocity and spectrum width increased smoothly from the cloud

478   top to base, suggesting that larger cloud droplets and broader size distributions exist near the cloud

479   base, which is attributable to more drizzle drops near the cloud base as illustrated in Fig. 7.

480   The vertical distributions of mixed-phase clouds in Figs. 11d-11f are similar to those of liquid

481   clouds. The more occurrences of larger reflectivity measurements and larger median values of

482   spectrum width near the cloud base are most likely due to the presence of moderate ice particles

483   and/or drizzle drops. The nearly same median values of reflectivity, Doppler velocity and spectrum

484   width (but slightly larger standard deviations in each level in mixed-phase clouds) in both liquid

485   and mixed-phase clouds suggest that the ice particle sizes in mixed-phase clouds are comparable

486   to cloud droplets and drizzle drops. The nearly uniform vertical distributions of Doppler velocity

487   and spectrum width indicate well-mixed liquid cloud droplets and ice particles throughout the

488   cloud layer in the mixed-phase clouds over NSO.

489   Compared to liquid and mixed-phase clouds, ice clouds had much lower reflectivities and

490   narrower spectrum width as shown in Figs. 11g-11i. Almost all reflectivity measurements were

491   less than -25 dBz with a median value of -35 dBz at the cloud base, resulting from small or

492   moderate ice particles but much lower concentration. A nearly constant Doppler velocity within

493   the cloud layer further supports the discussion of mixed-phase clouds above, i.e., the ice particle

494   sizes are independent of cloud height and comparable to liquid cloud droplets in the low-level

495   clouds over the SO. Because there are no mechanisms for growing large ice particles in such

496   shallow ice clouds, the accretion process cannot take place. From the statistical results in Fig. 7,

497   these ice particles have relatively little chance to become virga or raindrops and usually dissipate

498   or transition to other types of clouds.

499   Since there are not enough liquid cloud samples over the Polar region, only the mixed-phase

500   and ice clouds results are shown in Fig. 12. Compared to the vertical distributions of ice clouds

501   over NSO, the median values of reflectivity and Doppler spectrum width over SSO were lower

502   and narrower, indicating a lack of large ice particles in the Polar region. The small ice particles in

503   the Polar region were also reflected in their mixed-phase clouds. Compared to the vertical

504   distributions of the mixed-phased clouds over NSO, the median values of reflectivity and Doppler

505   spectrum width over SSO were dramatically lower (-35 dBz at SSO vs. -22 dBz at NSO; 0.25 m

506   s^{-1} at SSO vs. 0.32 m s^{-1} at NSO). Figure 12 illustrates that the ice particle sizes over SSO are

507   smaller, their size distributions are narrower than those over NSO, indicative of lack of large ice

508   particles over SSO.

509   **5. Summary and Conclusions**

510   In this study, we presented the statistical results of clouds over the Southern Ocean (SO), and

511   its northern (NSO) and southern (SSO) parts during MARCUS Intensive observational period

512   (IOP). We used the method developed in Xi et al., (2010) to calculate the occurrence frequencies

513   of different types of clouds and their corresponding cloud macrophysical properties. We developed

514   a new method to classify liquid, mixed-phased, and ice clouds in the single-layered low-level

515   clouds as well as their corresponding drizzling status. Lastly, we explored the meridional and

516   vertical distributions of these classified cloud properties. Analysis of the MARCUS cloud phase

517   and macrophysical properties has yielded the following conclusions.

518   1) The total cloud fractions (*CF*s) were 77.9 %, 67.6 %, and 90.3 % for the entire domain, NSO

519   and SSO, respectively, indicating that 22.7 % more clouds occurred in the Polar region than in

520   the mid-latitude region. The SSO had more clouds under 7 km, while the NSO had more clouds

521   above 7 km. Below 3 km, the occurrence frequencies of clouds over NSO decrease

522   dramatically from 37 % at an altitude of ~0.7 km to 16 % at 3 km, which is similar to the

523   vertical distributions of the low-level clouds over some Northern Hemisphere mid-latitude

524   regions, such as Eastern North Atlantic.

525   2) The single-layered low-level (LOW), deep connective or multi-layered (HML), and MOL

526   clouds are the three dominant types of clouds over the SO. Comparing the clouds between

527   NSO and SSO, all types of clouds in SSO are higher than those in NSO except HOL. The LOW

528   fraction, thickness, LWP over both NSO and SSO are comparable to each other. The mean

529   *LWP*s for LOW, MID and HOL clouds over NSO, range from ~130 to 150 g m^{-2}, while the

530   mean NSO *LWP*s (~270 g m^{-2}) for MOL and deep convective clouds (HML) are two times

531   higher than the same types of clouds over SSO. The mean *LWP*s of clouds over SSO are much

532   lower than the *LWP*s over NSO. Over the Southern Ocean, the single-layered or contiguous

533   clouds usually have higher LWP than their counterparts of multi-layered or non-contiguous

534   clouds. There are more non-contiguous HML and HOM than contiguous ones.

535   3) A new method was developed to classify liquid, mixed-phase and ice clouds in the single-

536   layered low-level clouds (LOW) based on comprehensive ground-based observations. The

537   mixed-phase clouds are dominant in the LOW cloud category with an occurrence frequency of

538   54.5 %. The 'OTHER' and ice clouds had similar occurrence frequencies of 18.1 % and 17.4 %,

539   respectively, while the liquid clouds had the least occurrence frequency of 10.1 %. The

540   percentages of non-drizzling, virga and drizzling for mixed-phase clouds were 50 %, 21 %,

541   and 29 %, and the drizzling frequencies of mixed-phase clouds strongly depend on H_{top}, that

542   is, higher drizzling frequencies occurred mostly at higher H_{top}.

543   4) The meridional distributions of H_{base}, H_{top} and ΔH are nearly independent on latitude, however,

544   their corresponding temperatures increased about 8 K from 69 °S to 43 °S. The meridional

545   variation of *LWP*s mimics that of cloud temperatures, having an increasing trend from south

546   to north. The mean *PWV* increased dramatically from ~ 5 mm at 69 °S to ~18 mm at 43 °S due

547   to increased sea surface and atmospheric temperatures. More liquid clouds occurred over NSO

548   but very few occurred over SSO, whereas more mixed-phase clouds occurred over SSO than

549   over NSO. There were no significant differences in ice clouds occurrences between NSO and

550   SSO.

551   5) The nearly same median values of reflectivity, Doppler velocity and spectrum width in both

552   liquid and mixed-phase clouds over NSO suggest that the ice particle sizes in mixed-phase

553   clouds are comparable to cloud droplets and drizzle drops. The uniform vertical distributions

554   of Doppler velocity and spectrum width suggest well-mixed liquid cloud droplets and ice

555   particles throughout the cloud layer in the mixed-phase clouds over NSO, which are quite

556   different from those over the DOE ARM NSA site where the liquid-topped mixed-phase low-

557   level clouds are common. The median values of reflectivity and Doppler spectrum width over

558   SSO were lower and narrower than those over NSO, indicating lack of large ice particles in

559   the polar region.

560   These results provide comprehensive statistical properties of all clouds over the SO during

561   MARCUS, including the occurrence frequencies of different types of clouds and their

562   corresponding cloud macrophysical properties. We also examined the meridional and vertical

563   distributions of the classified cloud properties. These statistics can be used as a ground truth to

564   evaluate satellite retrieved cloud properties and model simulations over the SO. The results of this

565   study will help to advance our understanding of the clouds over the SO, which may lead to

566   improved model simulations, as well as better representation of global climate.

567 *Data availability.* Data used in this study can be accessed from the DOE ARM's Data Discovery at

568 https://adc.arm.gov/discovery/

569

570 *Author contributions.* The idea of this study is discussed by BX, XD, and XZ. BX and XZ performed

571 the analyses and BX wrote the manuscript. BX, XD, XZ and PW participated in scientific discussions

572 and provided substantial comments and edits on the paper.

573

574 *Competing interests.* The authors declare that they have no conflict of interest.

575

576 *Acknowledgements.* The ground-based measurements were obtained from the Atmospheric

577 Radiation Measurement (ARM) Program sponsored by the U.S. Department of Energy (DOE)

578 Office of Energy Research, Office of Health and Environmental Research, and Environmental

579 Sciences Division. The data can be downloaded from http://www.archive.arm.gov/. Researchers

580 were supported by the NSF project under grant AGS-2031750 at the University of Arizona.

581 Specially thanks to Mr. Xingyu Zhang for providing analysis from CDP and 2DS microphysical

582 sensors during SOCRATES and Dr. Dale Ward for proofreading this manuscript.

583 **References.**

584 Albrecht, B. A.: Aerosols, cloud microphysics, and fractional cloudiness, Science,

585   doi:10.1126/science.245.4923.1227, 1989.

586 Bodas-Salcedo, A., Mulcahy, J. P., Andrews, T., Williams, K. D., Ringer, M. A., Field, P. R. and

587   Elsaesser, G. S.: Strong Dependence of Atmospheric Feedbacks on Mixed-Phase

588   Microphysics and Aerosol-Cloud Interactions in HadGEM3, J. Adv. Model. Earth Syst.,

589   doi:10.1029/2019MS001688, 2019.

590 Bony, S., Stevens, B., Frierson, D. M. W., Jakob, C., Kageyama, M., Pincus, R., Shepherd, T. G.,

591   Sherwood, S. C., Siebesma, A. P., Sobel, A. H., Watanabe, M. and Webb, M. J.: Clouds,

592   circulation and climate sensitivity, Nat. Geosci., doi:10.1038/ngeo2398, 2015.

593 Chubb, T. H., Jensen, J. B., Siems, S. T. and Manton, M. J.: In situ observations of supercooled

594   liquid clouds over the Southern Ocean during the HIAPER Pole-to-Pole Observation

595   campaigns, Geophys. Res. Lett., doi:10.1002/grl.50986, 2013.

596 Dong, X., Xi, B., Kennedy, A., Minnis, P. and Wood, R.: A 19-month record of marine aerosol-

597   cloud-radiation properties derived from DOE ARM mobile facility deployment at the

598   Azores. Part I: Cloud fraction and single-layered MBL cloud properties, J. Clim.,

599   doi:10.1175/JCLI-D-13-00553.1, 2014.

600 Hu, Y., Rodier, S., Xu, K. M., Sun, W., Huang, J., Lin, B., Zhai, P. and Josset, D.: Occurrence,

601   liquid water content, and fraction of supercooled water clouds from combined

602   CALIOP/IIR/MODIS measurements, J. Geophys. Res. Atmos.,

603   doi:10.1029/2009JD012384, 2010.

604 Intrieri, J. M., Fairall, C. W., Shupe, M. D., Persson, P. O. G., Andreas, E. L., Guest, P. S. and

605   Moritz, R. E.: An annual cycle of Arctic surface cloud forcing at SHEBA, J. Geophys. Res.

606   Ocean., doi:10.1029/2000jc000439, 2002.

607 Klein, S. A., Hall, A., Norris, J. R. and Pincus, R.: Low-Cloud Feedbacks from Cloud-Controlling

608   Factors: A Review, Surv. Geophys., doi:10.1007/s10712-017-9433-3, 2017.

609 Kalesse, H., de Boer, G., Solomon, A., Oue, M., Ahlgrimm, M., Zhang, D., Shupe, M. D., Luke,

610   E. and Protat, A.: Understanding rapid changes in phase partitioning between cloud liquid

611   and ice in stratiform mixed-phase clouds: An arctic case study, Mon. Weather Rev.,

612   doi:10.1175/MWR-D-16-0155.1, 2016.

613 Lang, F., Huang, Y., Siems, S. T. and Manton, M. J.: Characteristics of the Marine Atmospheric

614   Boundary Layer Over the Southern Ocean in Response to the Synoptic Forcing, J. Geophys.

615   Res. Atmos., doi:10.1029/2018JD028700, 2018.

616 Listowski, C., Delanoë, J., Kirchgaessner, A., Lachlan-Cope, T. and King, J.: Antarctic clouds,

617   supercooled liquid water and mixed phase, investigated with DARDAR: Geographical and

618   seasonal variations, Atmos. Chem. Phys., doi:10.5194/acp-19-6771-2019, 2019.

619 Mace, G. G., Zhang, Q., Vaughan, M., Marchand, R., Stephens, G., Trepte, C. and Winker, D.: A

620   description of hydrometeor layer occurrence statistics derived from the first year of merged

621   Cloudsat and CALIPSO data, J. Geophys. Res. Atmos., doi:10.1029/2007JD009755, 2009.

622 Mace, G. G. J. and Protat, A.: Clouds over the Southern Ocean as observed from the R/V

623   investigator during CAPRICORN. Part I: Cloud occurrence and phase partitioning, J. Appl.

624   Meteorol. Climatol., doi:10.1175/JAMC-D-17-0194.1, 2018.

625 Mace, G. G., Protat, A., Humphries, R. S., Alexander, S. P., McRobert, I. M., Ward, J., Selleck,

626   P., Keywood, M. and McFarquhar, G. M.: Southern Ocean Cloud Properties Derived From

627   CAPRICORN and MARCUS Data, J. Geophys. Res. Atmos., doi:10.1029/2020JD033368,

628   2021.

629 Marchand, R., Ackerman, T., Westwater, E. R., Clough, S. A., Cady-Pereira, K. and Liljegren, J.

630   C.: An assessment of microwave absorption models and retrievals of cloud liquid water

631   using clear-sky data, J. Geophys. Res. Atmos., doi:10.1029/2003jd003843, 2003.

632 Marchand, R., Wood, R., Bretherton, C., McFarquhar, G., Protat, A., Quinn, P., Siems, S., Jakob,

633   C., Alexander, S., Weller, B.: The Southern Ocean Clouds, Radiation Aerosol Transport

634   Experimental   Study   (SOCRATES),   whitepaper   available   from

635   http://www.atmos.washington.edu/socrates/SOCRATES_white_paper_Final_Sep29_201

636   4.pdf, 2014.

637 Mccoy, D. T., Hartmann, D. L. and Grosvenor, D. P.: Observed Southern Ocean cloud properties

638   and shortwave reflection. Part II: Phase changes and low cloud feedback, J. Clim.,

639   doi:10.1175/JCLI-D-14-00288.1, 2014.

640 McFarquhar, G., Bretherton, C., Alexander, S., DeMott, P., Marchand, R., Protat, A., Quinn, P.,

641   Siems, S., Weller, R., Wood, R.: Measurements of Aerosols, Radiation, and Clouds over

642   Sothern Ocean (MARCUS) Science Plan, DOE ARM Climate Research Facility.,

643   DOE/SC-ARM-16-011, available at: http://arm.gov/publications/programdocs/doe-sc-

644   arm-16-011.pdf, 2016.

645 McFarquhar, G and coauthors, 2021; Observations of Clouds, Aerosols, Precipitation, and
646
647   Surface Radiation over the Southern Ocean An Overview of CAPRICORN, MARCUS,
648
649   MICRE, and SOCRATES. BAMS, https://doi.org/10.1175/BAMS-D-20-0132.2.
650
651 Mohrmann, J., Finlon, J., Atlas, R., Lu, J., Hsiao, I., Wood, R.: University of Washington Ice-

652   Liquid Discriminator single particle phase classifications and 1 Hz particle size

653   distributions/heterogeneity estimate, Version 1.0. UCAR/NCAR - Earth Observing

654   Laboratory., doi:10.26023/PA5W-4DRX-W50A, Last Access: Nov 01, 2021

655   Morrison, H., De Boer, G., Feingold, G., Harrington, J., Shupe, M. D. and Sulia, K.: Resilience of

656   persistent Arctic mixed-phase clouds, Nat. Geosci., doi:10.1038/ngeo1332, 2012.

657   Muradyan, P. and Coulter, R.: Micropulse Lidar (MPL) Instrument Handbook. DOE ARM Climate

658   Research Facility, DOE/SC-ARM-TR-019, 2020. Available at:

659   https://www.arm.gov/publications/tech_reports/handbooks/mpl_handbook.pdf, last access:

660   25 March 2022.

661   Qiu, S., Dong, X., Xi, B. and Li, J. L. F.: Characterizing Arctic mixed-phase cloud structure and

662   its relationship with humidity and temperature inversion using ARM NSA observations, J.

663   Geophys. Res., doi:10.1002/2014JD023022, 2015.

664   Rémillard, J., Kollias, P., Luke, E., and Wood, R.: Marine Boundary Layer Cloud Observations in

665   the Azores, J. Climate, 25, 7381-7398, 10.1175/JCLI-D-11-00610.1, 2012.

666   Sassen, K.: The polarization lidar technique for cloud research: a review and current assessment,

667   Bull. - Am. Meteorol. Soc., doi:10.1175/1520-0477(1991)072<1848:TPLTFC>2.0.CO;2,

668   1991.

669   Shupe, M. D., Uttal, T. and Matrosov, S. Y.: Arctic cloud microphysics retrievals from surface-

670   based remote sensors at SHEBA, J. Appl. Meteorol., doi:10.1175/JAM2297.1, 2005.

671   Shupe, M.: A ground-based multisensory cloud phase classifier, Geophys. Res. Lett.,

672   doi:10.1029/2007GL031008, 2007.

673   Stanfield, R. E., Dong, X., Xi, B., Kennedy, A., Del Genio, A. D., Minnis, P. and Jiang, J. H.:

674   Assessment of NASA GISS CMIP5 and Post-CMIP5 Simulated Clouds and TOA

675   Radiation Budgets Using Satellite Observations. Part I: Cloud Fraction and Properties, J.

676   Clim., doi:10.1175/jcli-d-13-00558.1, 2014.

677 Stanfield, R. E., Dong, X., Xi, B., Del Genio, A. D., Minnis, P., Doelling, D. and Loeb, N.:

678   Assessment of NASA GISS CMIP5 and post-CMIP5 simulated clouds and TOA radiation

679   budgets using satellite observations. Part II: TOA radiation budget and CREs, J. Clim.,

680   doi:10.1175/JCLI-D-14-00249.1, 2015.

681 Stocker, T. F., Qin, D., Plattner, G. K., Tignor, M. M. B., Allen, S. K., Boschung, J., Nauels, A.,

682   Xia, Y., Bex, V. and Midgley, P. M.: Climate change 2013 the physical science basis:

683   Working Group I contribution to the fifth assessment report of the intergovernmental panel

684   on climate change., 2013.

685 Toto, T. and Jensen, M.: Interpolated Sounding and Gridded Sounding Value-Added Products.

686   DOE ARM Climate Research Facility, DOE/SC-ARM-TR-183, 2016. Available at:

687   https://www.arm.gov/publications/tech_reports/doe-sc-arm-tr-183.pdf, last access: 25

688   March 2022.

689 Uin, J.: Cloud Condensation Nuclei Particle Counter Instrument Handbook. DOE ARM Climate

690   Research Facility, DOE/SC-ARM-TR-168, 2016. Available at:

691   https://www.arm.gov/publications/tech_reports/handbooks/ccn_handbook.pdf, last access:

692   25 March 2022.

693 Wu, P., Dong, X. and Xi, B.: Marine boundary layer drizzle properties and their impact on cloud

694   property retrieval, Atmos. Meas. Tech., doi:10.5194/amt-8-3555-2015, 2015.

695 Wu, P., Dong, X., Xi, B., Liu, Y., Thieman, M. and Minnis, P.: Effects of environment forcing on

696   marine boundary layer cloud-drizzle processes, J. Geophys. Res.,

697   doi:10.1002/2016JD026326, 2017.

698 Wu, P., Dong, X. and Xi, B.: A climatology of marine boundary layer cloud and drizzle properties

699   derived from ground-based observations over the azores, J. Clim., doi:10.1175/JCLI-D-20-

700   0272.1, 2020.

701 Xi, B., Dong, X., Minnis, P. and Khaiyer, M. M.: A 10 year climatology of cloud fraction and

702   vertical distribution derived from both surface and GOES observations over the DOE ARM

703   SPG site, J. Geophys. Res. Atmos., doi:10.1029/2009JD012800, 2010.

704 Zelinka, M. D., Myers, T. A., McCoy, D. T., Po-Chedley, S., Caldwell, P. M., Ceppi, P., Klein, S.

705   A. and Taylor, K. E.: Causes of Higher Climate Sensitivity in CMIP6 Models, Geophys.

706   Res. Lett., doi:10.1029/2019GL085782, 2020.

707 Zhao, L., Zhao, C., Wang, Y., Wang, Y. and Yang, Y.: Evaluation of Cloud Microphysical

708   Properties Derived From MODIS and Himawari-8 Using In Situ Aircraft Measurements

709   Over the Southern Ocean, Earth Sp. Sci., doi:10.1029/2020EA001137, 2020.

Table 1. ARM AMF2 instruments and their corresponding measurements and uncertainties used in this study

Parameter	Instruments/ Methods	Uncertainty	References
Cloud-base height	Ceilometer/MPL	15 m	Rémillard et al., 2012
Cloud-top height	95 GHz cloud radar	43 m	Rémillard et al., 2012
Cloud-base and -top temps	Radiosonde sounding	0.2 °C	Toto and Jensen, 2016
Profiles of reflectivity, Doppler velocity and Spectra	W-band ARM Cloud Radar (WACR), 95 GHz	Sensitivity: -50 dBZ at 2 km	Rémillard et al., 2012
linear depolarization ratios (*LDR*) and backscatter	Micropulse lidar, MPL Liquid: LDR<0.11 Mix: 0.11<LDR<0.15 Ice: LDR> 0.15		Shupe et al. 2005 Muradyan and Coulter, 2020
Cloud LWP	Microwave radiometer	~15-30 g m^{-2} Physical retrieval	Marchand et al., 2003
CCN and aerosol properties	Aerosol Observing System	1-min resolution; Uncertainties < 10%	Uin, 2016

Table 2. Mean, standard deviation, minimum and maximum cloud-base heights (H_{base}), -top heights (H_{top}), and *LWP*s (all samples, single-layered, multilayered) of all seven types of clouds over the SO. All cloud heights have a unit of kilometer, and *LWP* has a unit of g m^{-2}

	LOW	MID	MOL	HGH	HOM	HML	HOL
$H_{base} \pm$ **std** min, max	0.92 ± 0.57 0.06, 2.86	4.14 ± 0.61 3.00, 5.84	1.37 ± 0.96 0.06, 5.27	8.51 ± 2.23 6.00, 18.67	4.70 ± 0.80 3.01, 7.72	1.22 ± 0.98 0.06, 7.81	1.14 ± 1.12 0.07, 10.37
$H_{top} \pm$ **std** min, max	1.62 ± 0.63 0.29, 3.0	4.88 ± 0.68 3.17, 6.0	4.29 ± 0.89 1.39, 5.99	9.75 ± 2.13 6.20,18.79	7.93 ± 1.27 5.47, 17.98	7.81 ± 1.35 3.62,17.38	8.93 ± 1.66 1.79, 17.56
LWP $\pm$ **std** Max *LWP*	122.4±134.2 1470.8	86.7±124.5 501.1	168.7±236.7 1937.1	/ /	40.9±40.8 345.7	169.2±238.4 1819.3	129.8±202. 1785.2
LWP $\pm$ **std** **(single layer)** max	126.6±138.1 1470.8	88.7±128.9 501.1	193.1±271.9 1937.1	/ /	48.7±51.7 345.7	270.8±349.5 1819.3	/ /
LWP $\pm$ **std** **(multi-layer)** max	96.2±103.4 842.3	77.2±109.2 305.6	139.0±180.7 1830.2	/ /	32.3±21.3 86.8	148.4±202.4 1690.7	129.8±202. 1785.2
Multi-layer percentage %	18.1	39.6	50.0	44.9	73.1	77.7	100

* The definition of the cloud types as follow: LOW (H_{base} and $H_{top} \leq 3\ km$); MID ($H_{base} > 3\ km$ and $H_{top} \leq 6\ km$); HGH ($H_{base} > 6\ km$); MOL ($H_{base} < 3\ km$ and $H_{top} \leq 6\ km$); HOM ($3\ km < H_{base} < 6\ km$ and $H_{top} > 6\ km$); HML ($H_{base} < 3\ km$, $H_{top} \geq 6\ km$ with a MID layer); HOL (LOW and HGH appear at the same time).

Table 3a. Comparison of cloud phase identifications between our classification method and Shupe et al. (2005) method in each 5-min measurements, the unit is number of 5-min samples

Shupe \this study	Liquid (this study)	Mixed-phase (this study	Ice (this study)
Liquid	468	490	0
Mixed-phase	98	3840	0
Ice	81	0	1195

*Numbers denote the cloud sample classifications between two methods. For example, the number 98 denote a total of 98 samples are classified as Mixed-phase using Shupe's method, while are classified as Liquid using this study's method.

Table 3b. The cloud phase partitioning from CDP and 2DS during SOCRATES

Phase partitioning	1 second	10 seconds	30 seconds
Samples #	27,280	2,255	836
Liquid, %	58.8	26.2	18.8
Mixed-phase, %	38.9	69.1	77.0
Ice, %	2.3	4.7	4.2

Note that Cloud Droplet Probe (CDP) measures particle size from 2 to 50 um in diameter; Two-Dimensional Stereo Probe (2DS) measures particle size from 50 to 5000 um in diameter.

Table 4. Liquid, mixed, ice and OTHER phases of cloud properties within the single-layered low-level clouds

Phase	Samples	H_{base}, km	H_{top}, km	ΔH, km	LWP, g m^{-2}	PWV, mm
Liquid	697	0.424±0.204	1.327±0.242	0.903	113.6±90.1	15.7±3.5
Mixed	3777	0.834±0.465	1.434±0.617	0.587	119.7±136.6	8.9±5.0
Ice	1205	1.218±0.635	1.737±0.651	0.519	0	8.4±4.5
OTHER	1255	0.700±0.454	1.774±0.571	1.074	141.9±137.5	11.4±5.9
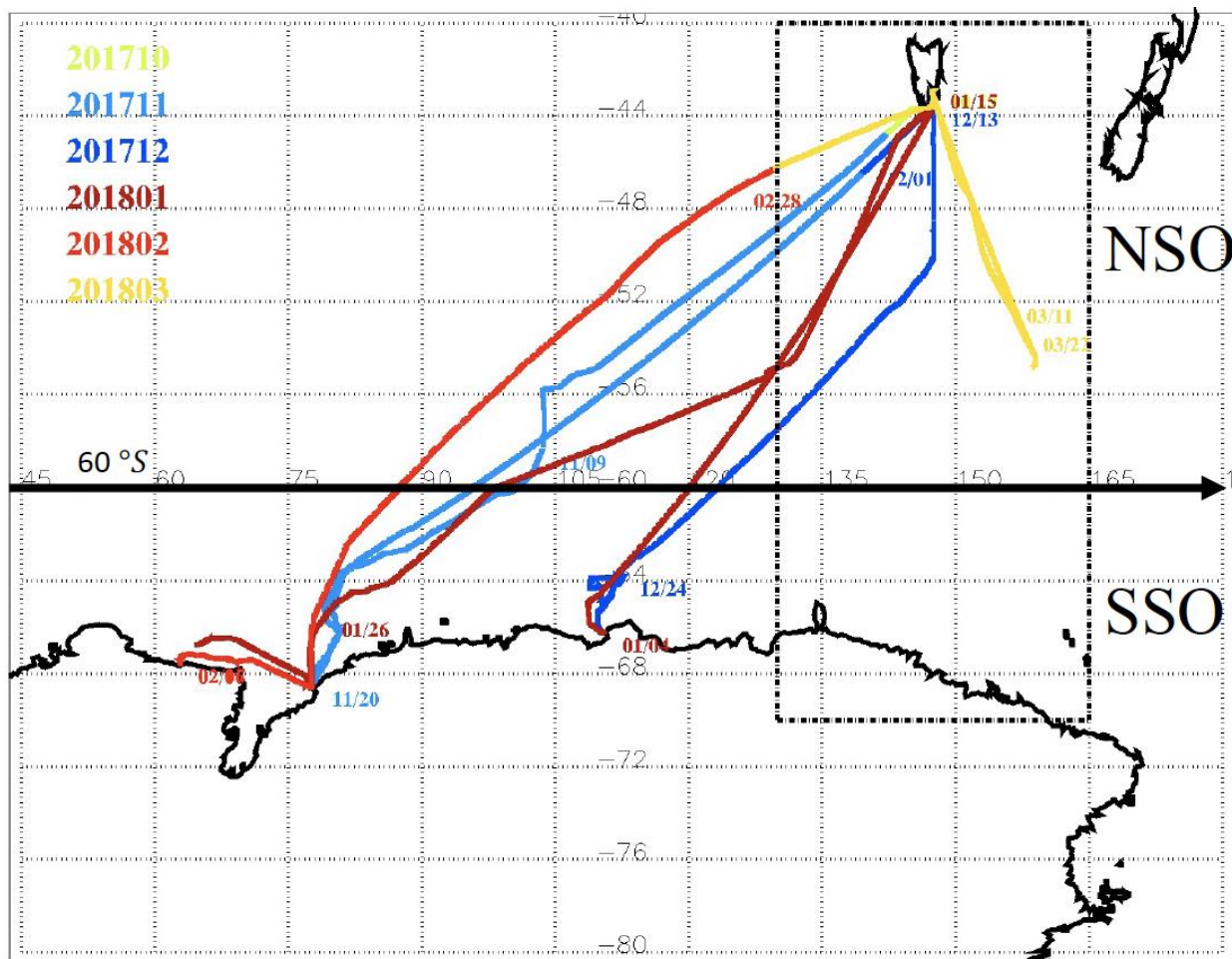
Figure 1. Shiptrack measurements between Hobart, Australia and Antarctica. Different colors represent different month's shiptracks from Oct. 29, 2017 to Mar. 23, 2018 during MARCUS. Along the shiptracks, the study domain is separated into northern (NSO) and southern (SSO) parts of the Southern Ocean with a demarcation line of 60 °S in order to study the clouds over the mid-latitudes (North of 60 °S) and Polar region (South of 60 °S). The black dotted rectangle represents the SOCRATES study domain. Some of the dates are labeled along the shiptracks, indicating the direction of the ship.
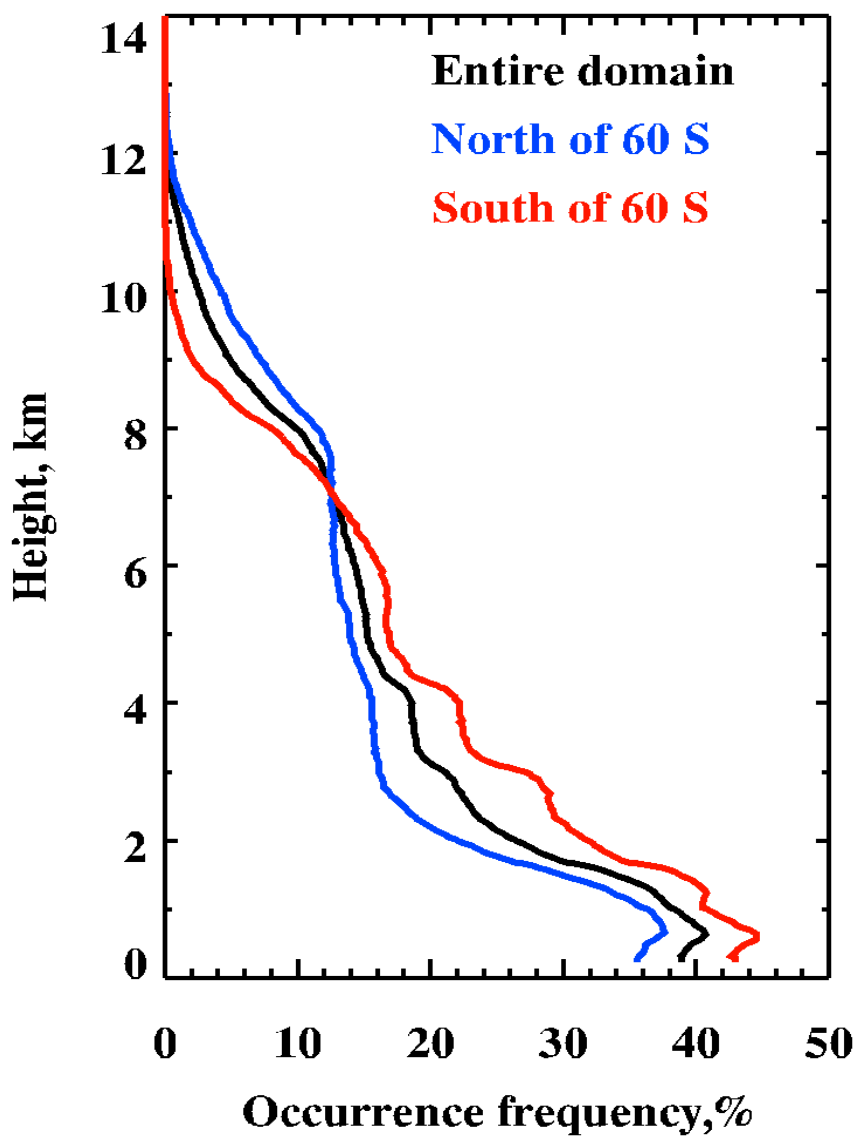
Figure 2. Mean vertical distributions of total clouds derived from ARM radar-lidar observations with a 5-min temporal resolution and a 30-m vertical resolution during MARCUS.
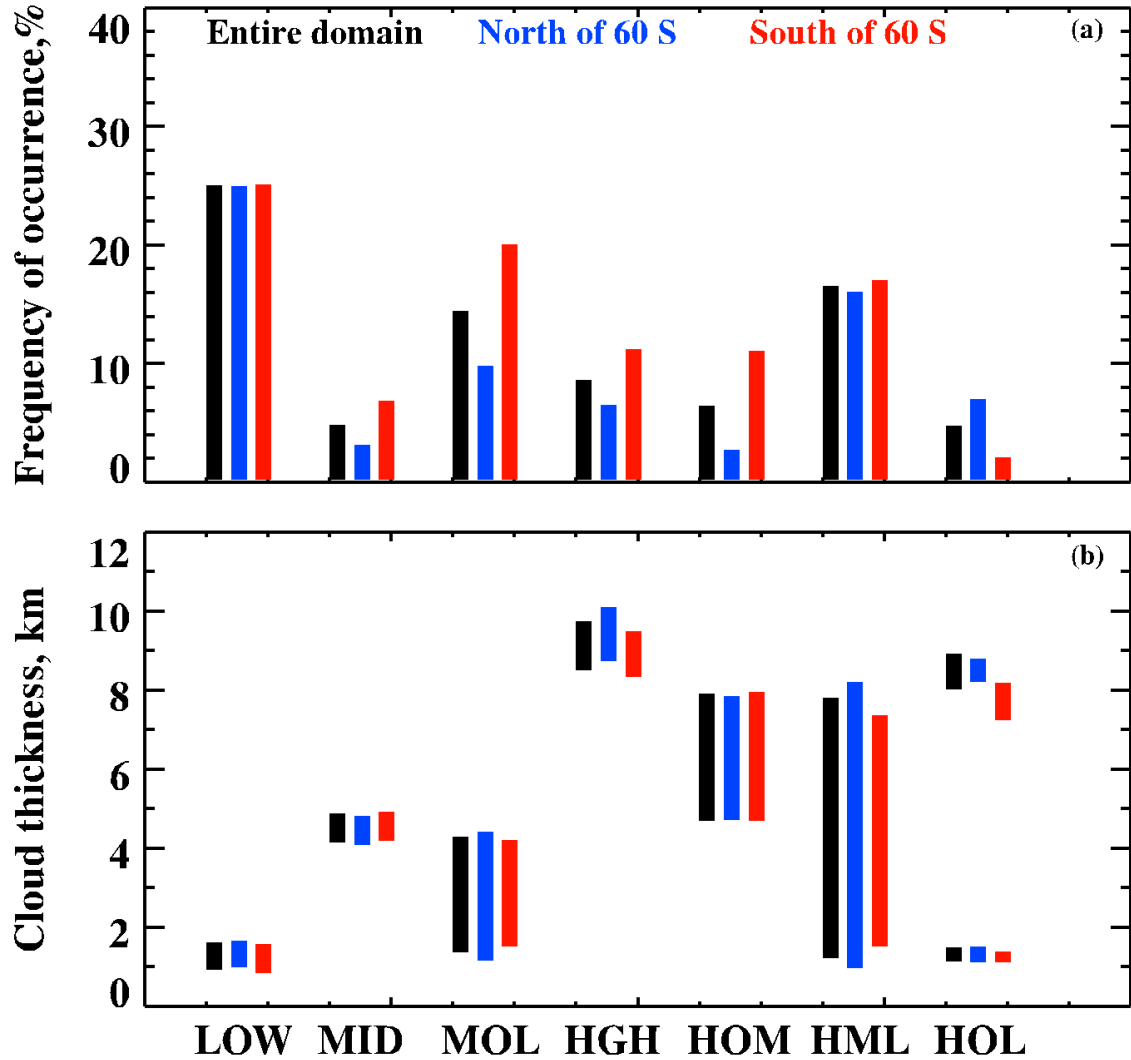
Figure 3. (a) Occurrence frequencies of categorized clouds by their vertical structures. LOW, single‑layered low clouds (H_{base} and $H_{top} \leq 3\ km$); MID, singlelayered middle clouds ($H_{base} > 3\ km$ and $H_{top} \leq 6\ km$); MOL, MID over LOW ($H_{base} < 3\ km$ and $H_{top} \leq 6\ km$); HGH, singlelayered high clouds ($H_{base} > 6\ km$); HOM, HGH over MID ($3\ km < H_{base} < 6\ km$ and $H_{top} > 6\ km$); HML, HGH over MID and LOW ($H_{base} < 3\ km$, $H_{top} \geq 6\ km$ with a MID layer); and HOL, HGH over LOW (LOW and HGH appear at the same time). (b) Cloud thickness for each type of clouds (bar), the top and bottom of the bar represent the maximum cloud-top and minimum cloud-base heights, respectively. Black, blue, and red bars represent the entire domain (Lat:41-69 °S; Long: 60-160° E), north of 60 °S (NSO), and south of 60°S (SSO), respectively, during the MARCUS field campaign (10/2017-3/2018).
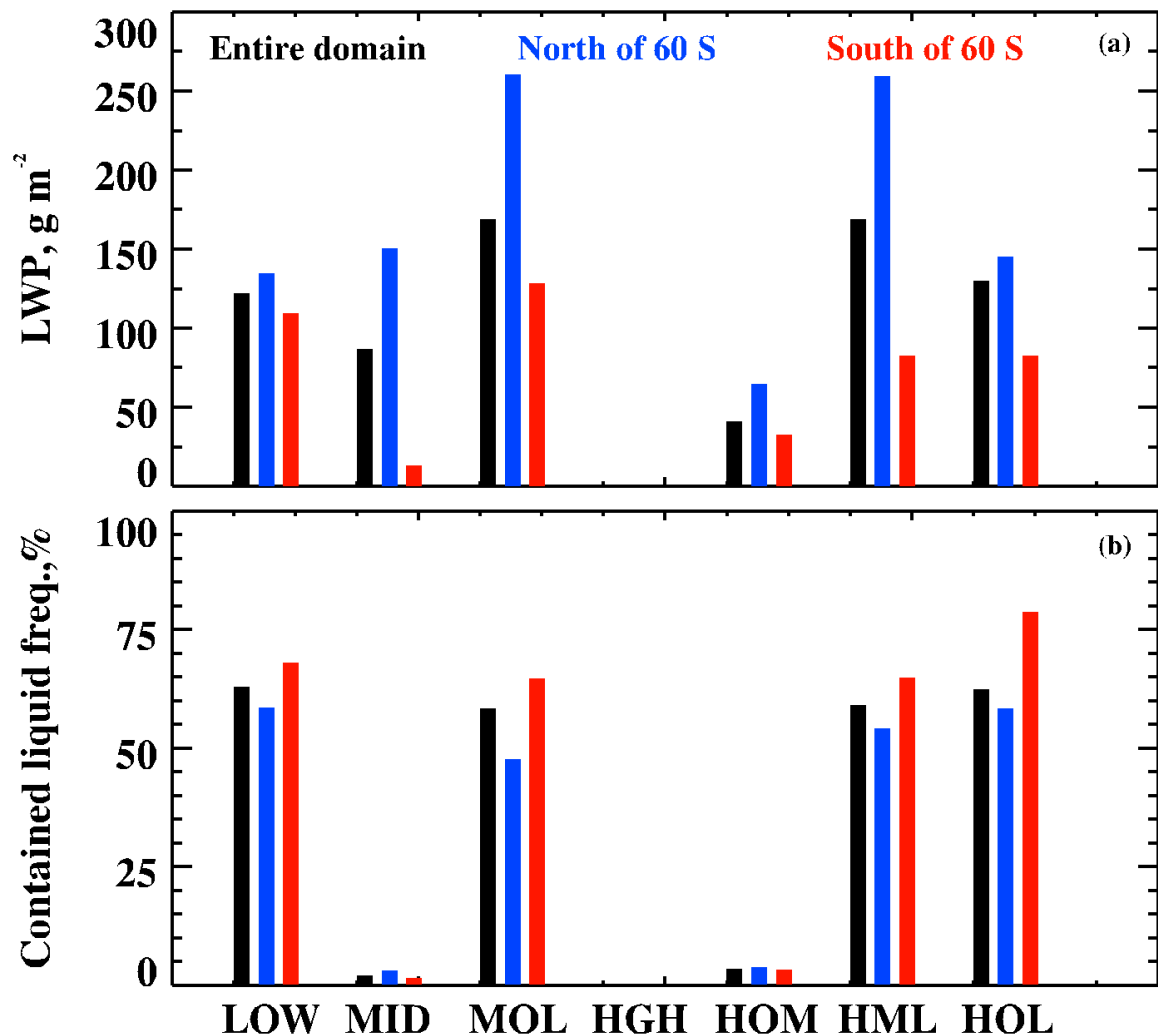
Figure 4. (a) Cloud liquid water paths (*LWP*s) retrieved from microwave radiometer (MWR) measured brightness temperatures using a physical retrieval method for each type of cloud. (b) The occurrence frequencies of LWPs> 10 gm^{-2} for each type of clouds

Phase classification algorithm for single layered low level clouds
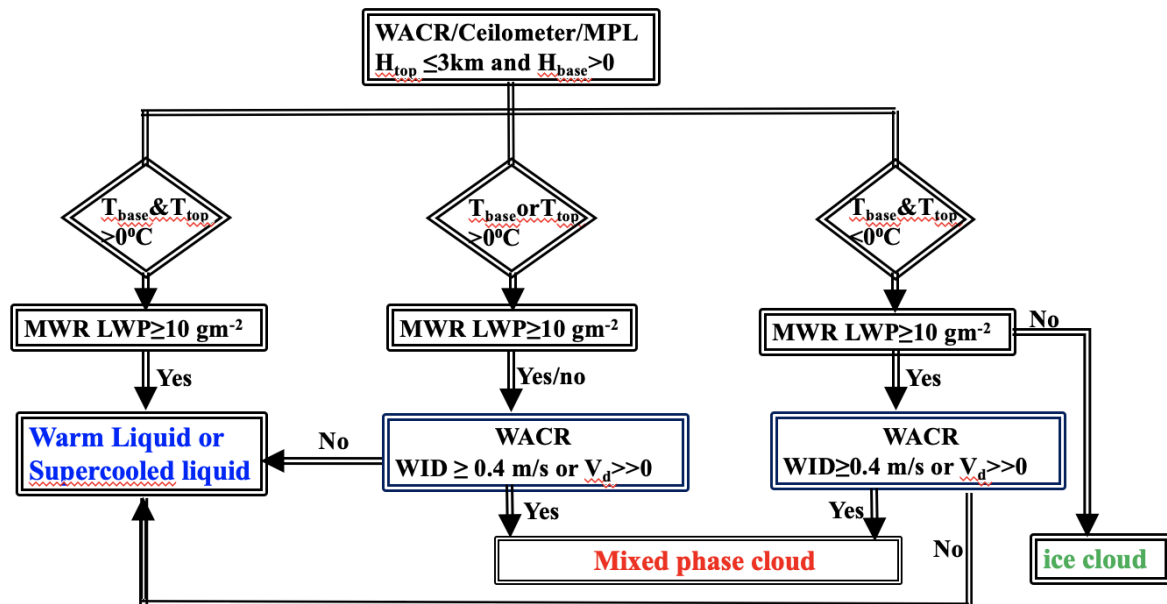
Figure 5. A flow chart for phase classification of single-layered low-level clouds. W-Band (95 GHz) ARM Cloud Radar (WACR) provides radar spectrum width (*WID*) and Doppler velocity (V_d).
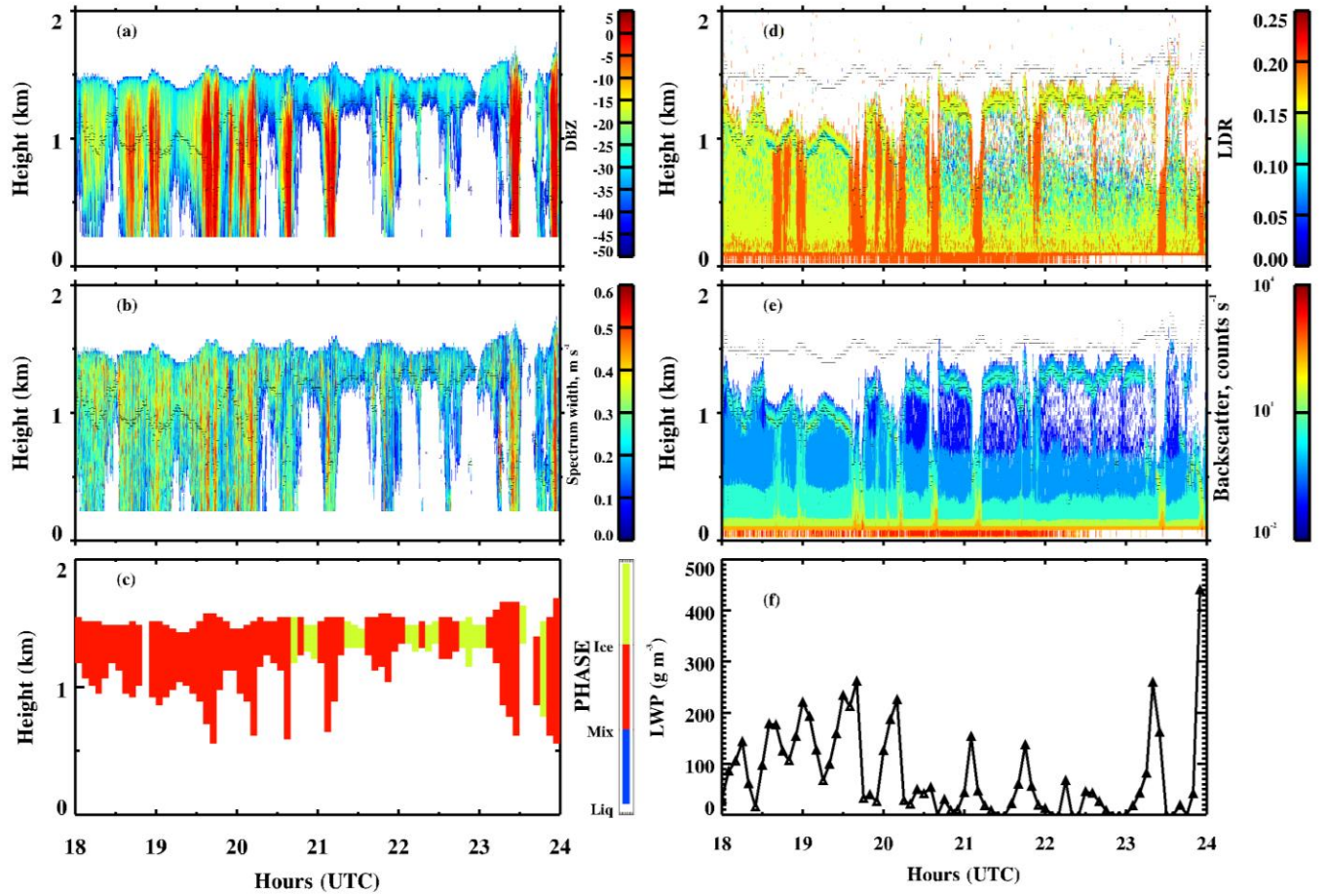
Figure 6. A case study that shows our phase classification (left column) and MicroPulse Lidar (MPL) linear depolarization ratios (*LDR*) and backscatter. W-Band (95 GHz) ARM Cloud Radar (WACR) reflectivity is shown in (a) and spectrum width is shown in (b). Correspondingly, the phase classification in (c); MPL *LDR* in (d) and backscatter in (e); and MWR-derived *LWP* in (f).
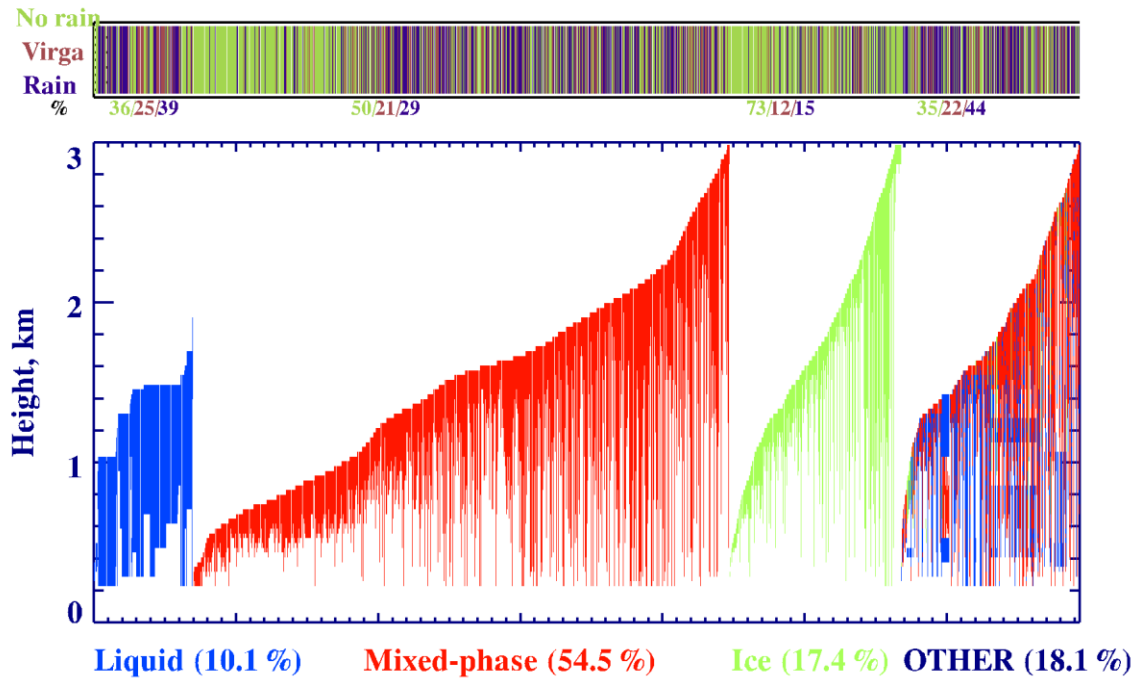
Figure 7. (Upper Panel) The drizzling status for each categorized cloud type, e.g., no rain (yellow-green), virga (brown) and rain (navy blue), the percentages shown below the x-axis represent the portion of drizzling in each type of clouds. (Bottom Panel) The percentages and vertical distributions of classified liquid, mixed-phase, ice, and 'OTHER' clouds for each column in the single-layered low-level clouds, represented by different colors, over the entire domain during MARCUS. Each line represents one 5-min sample. The definition of drizzle here is the radar reflectivity below the ceilometer-derived cloud base, which could be either liquid drizzle drops or ice crystals.
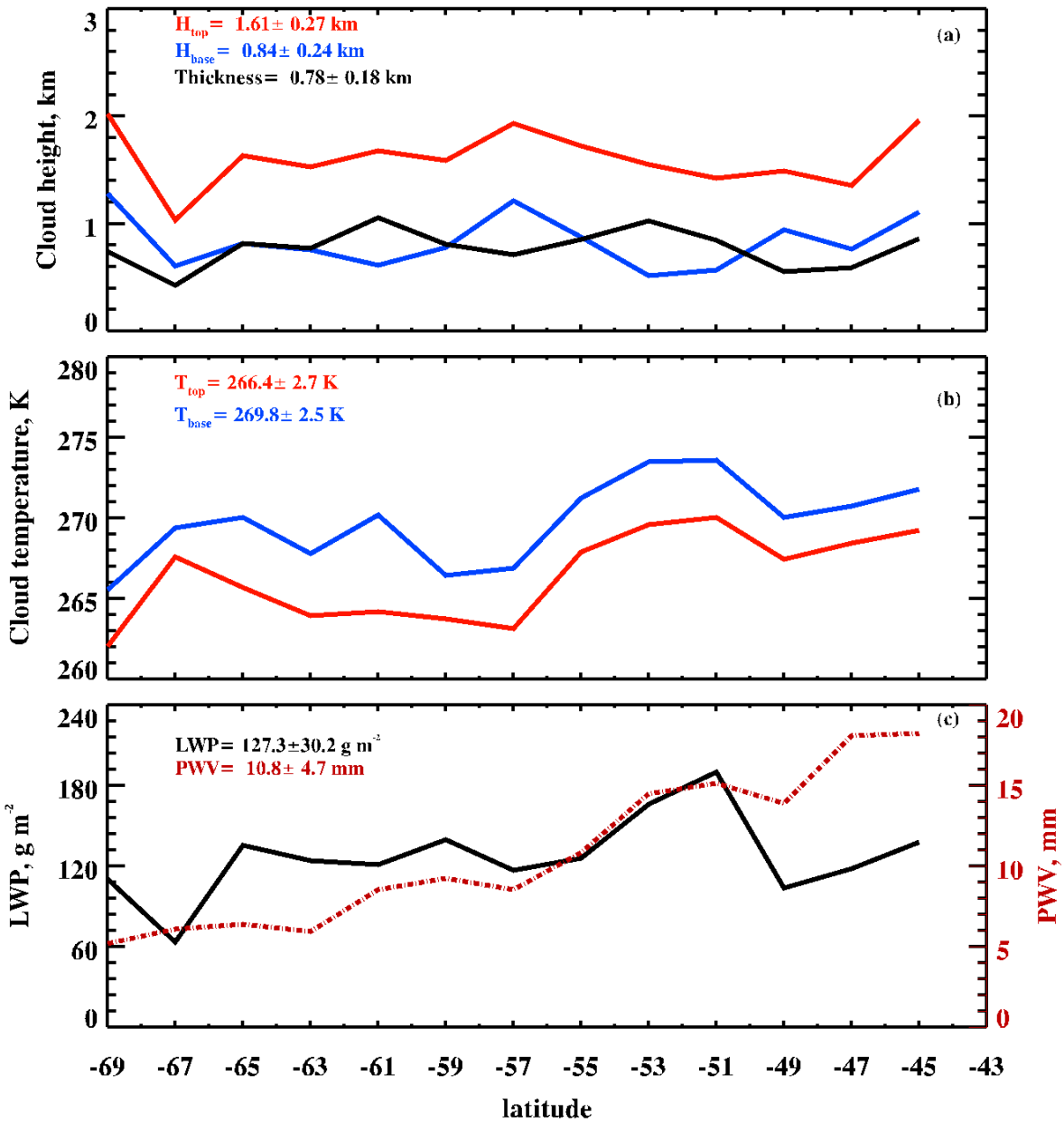
Figure 8. Meridional variations of single-layered low-level cloud properties: (a) cloud-base (H_{base}) and -top (H_{top}) heights, and cloud thickness (ΔH), (b) cloud-base (T_{base}) and -top (T_{top}) temperatures, and (c) cloud liquid water path (*LWP*) and precipitable water vapor (PWV) over the entire domain during MARCUS.
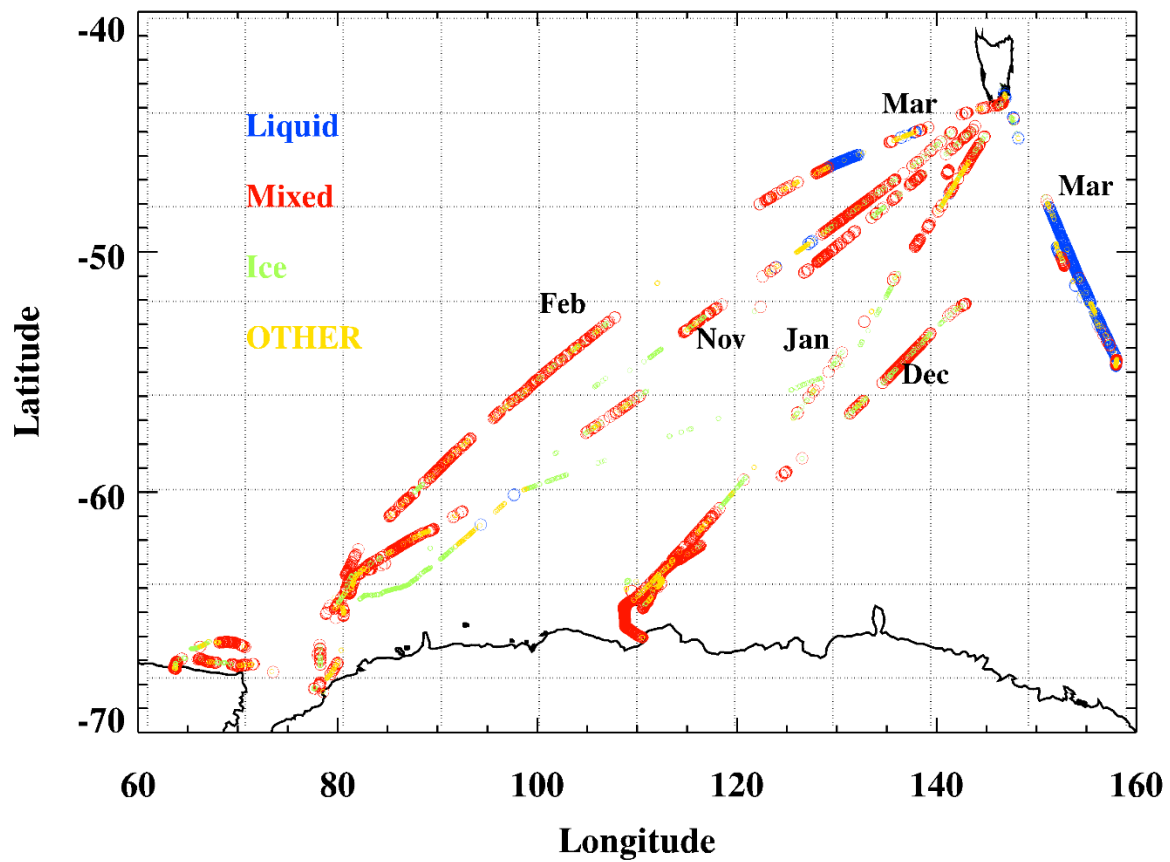
Figure 9. The latitudinal and longitudinal distributions of classified mixed-phase, liquid, and ice clouds in the single-layered low-level clouds. The liquid (blue), mixed (red), ice (light green), and OTHER (yellow) are shown along each shiptrack from October 2017 to March 2018 during MARCUS.
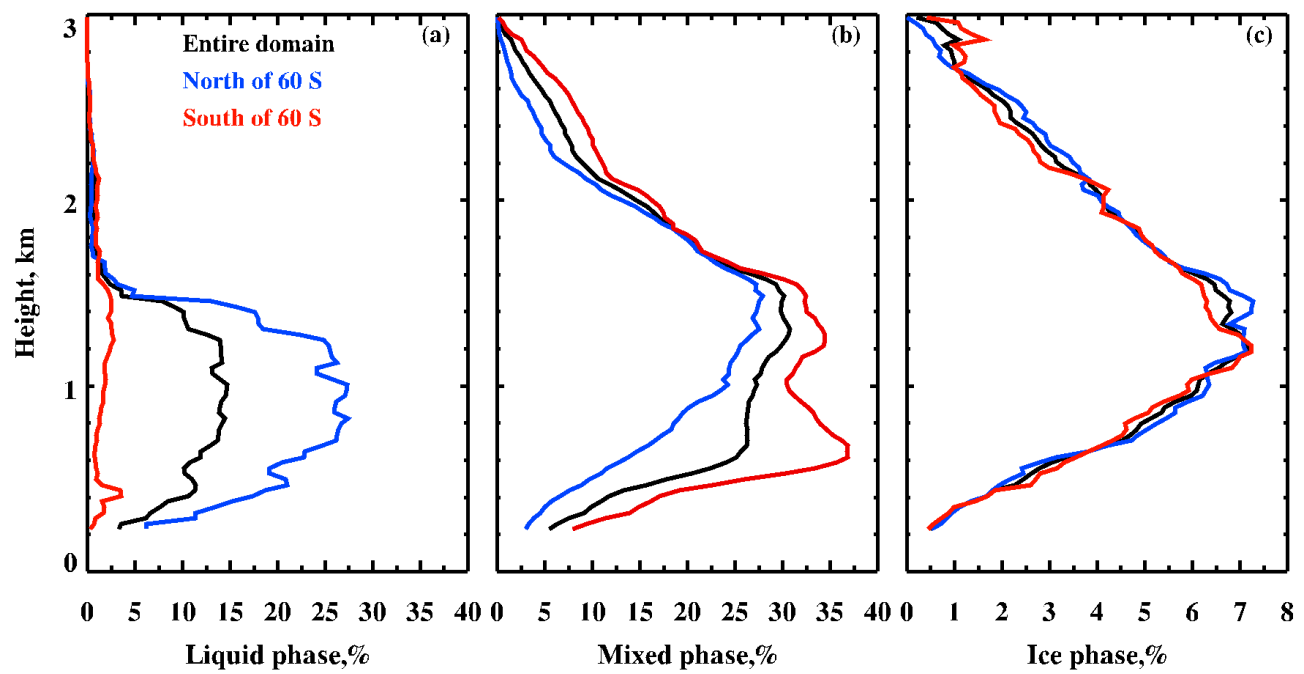
Figure 10. Occurrence frequencies of classified mixed-phase, liquid, and ice clouds over the entire domain (black), North of 60 °S (blue) and South of 60 °S (red) during MARCUS.
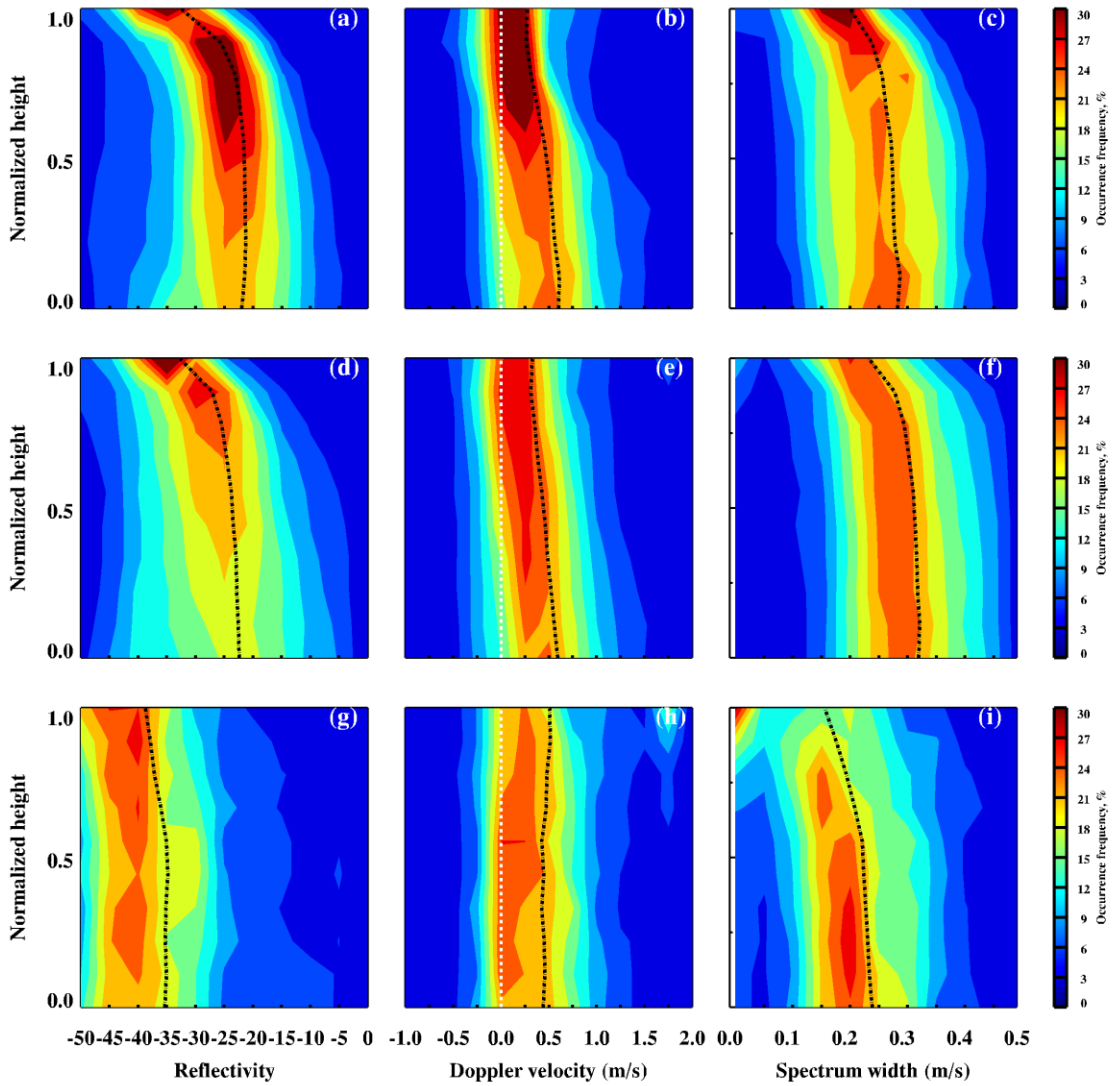
Figure 11. Normalized vertical distributions of radar reflectivity (a), Doppler velocity (b) and spectrum width (c) for the classified liquid (upper panel), mixed-phase (d to f, middle panel) and ice (g to i, bottom panel) clouds over the North of 60 °S during MARCUS Intensive observational period (IOP). Normalized height is defined as $= \frac{H-H_{base}}{H_{top}-H_{base}}$ where cloud base is denoted as 0 and cloud top is 1. The black lines represent the median values and the white lines in Doppler velocity represent the reference of 0.0 m s^{-1}.
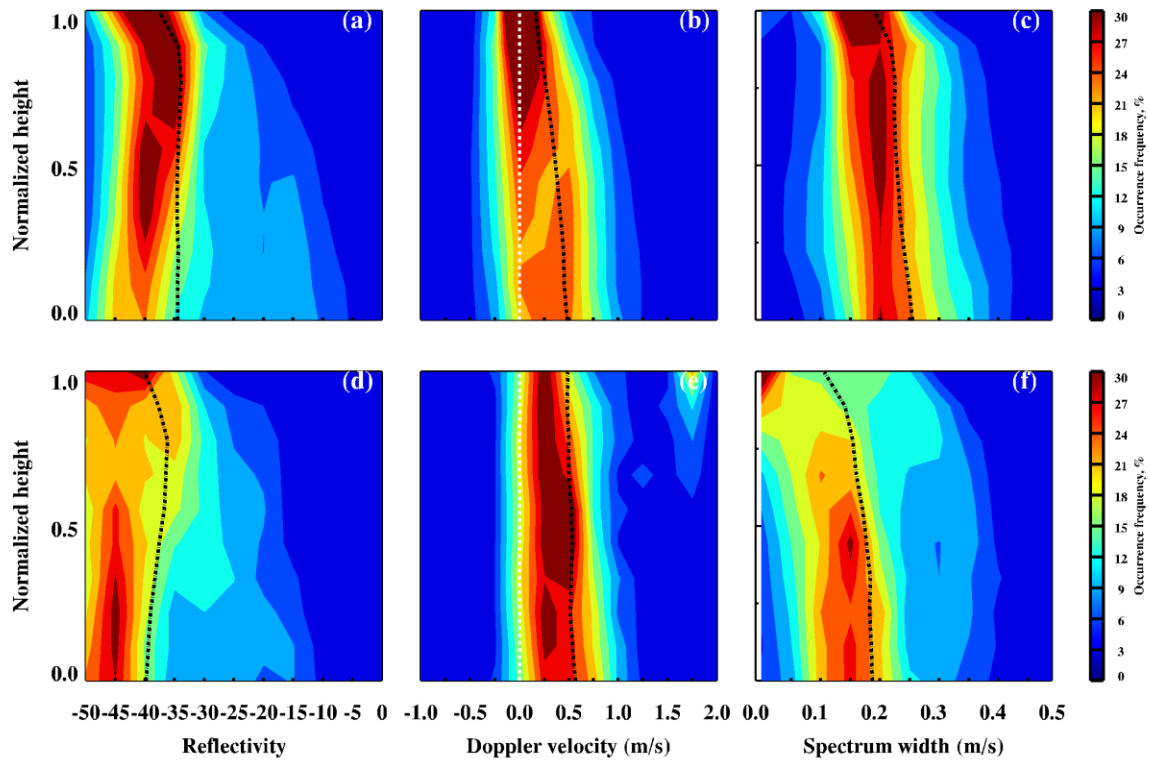
Figure 12. Same as Fig. 11 but only for mixed-phase (a to c, upper panel) and ice (d to f, bottom panel) over the south of 60 °S during MARCUS.